PHYSICAL REVIEW A VOLUME 24, NUMBER 5 NOVEMBER 1981

Shock waves in the Toda lattice: Analysis

Brad Lee Holian
Los Alamos National Laboratory, Los Alamos, New Mexico 87545

Hermann Flaschka and David W. McLaughlin*
Mathematics Department, University of Arizona, Tucson, Arizona 85721

(Received 1 December 1980)

Known analytical results are used to analyze molecular-dynamics experiments of shock waves in the one-dimensional Toda lattice. (This lattice provides a physically realistic model which contains the hard-sphere and harmonic lattices as limits.) Both explicit solutions and rather general theoretical properties have been employed. The leading edge of the shock front is well represented quantitatively by a single isolated soliton. Once compression is properly taken into account, the interior of the shock wave is accurately described by a slowly varying Toda wave train. A sharp transition in the dynamical response exists as the shock strength passes a critical value; this critical value is identified mathematically by the spectral transform for the Toda lattice. Finally, a local spectral transform is used to measure, directly from the numerical data, the wave-train characteristics of the shock profile.

I. INTRODUCTION

When a piston pushes steadily at velocity u_p on a real three-dimensional material, a shock wave travels out in front of the piston at velocity u_s. Between the shock front and the piston, the density, particle velocity, pressure, and internal energy of the shocked material are higher than in the unshocked material. The wave near the center of the piston can be thought of as being planar, or one dimensional, if edge effects are negligible. In many circumstances this planar shock wave has a steady profile which results from an effective dissipation, whose origin is particle flow in directions transverse to that of propagation. A shock wave can also be smoothed by dispersion, which does not, however, ensure that the wave will be steady.

In a one-dimensional world, dissipation due to transverse particle motion is, of course, impossible. Though dissipation could be introduced by artificial viscous damping in order to make the shock wave steady, dissipation is not necessary to *smooth* a shock wave, since dispersion by itself will do so. If a one-dimensional, dispersive chain is nonlinear, the nonlinearity will act with the dispersion to produce collective excitations (solitons and soliton wave trains) which smooth the shock wave and transport its energy down the chain.

In this paper we study shock waves in a particular one-dimensional, dispersive, nonlinear chain—the "Toda lattice." For the Toda lattice, analytical expressions are known for the solitons and soliton wave trains. Furthermore, there exists a nonlinear transformation from the positions and velocities of the particles in the chain to these collective coordinates. We study the structure of the Toda shock profile by using analytical expressions for the solitons and soliton wave trains, along with the theoretical transformation to these collective excitations, to analyze numerical representations of the shock profile. The experimental data were obtained from earlier molecular-dynamics computations.[1,2]

We summarize our results in terms of three regions of the shock profile: the *shock front*, the *rear of the shock* profile near the piston, and a *transition region* between the front and the rear. (1) The entire shock profile may be described as a slowly varying soliton wave train. (2) *Near the shock front*, the solitons in the train are far enough apart that they behave as isolated solitons. For small values of the piston velocity, these solitons are separating logarithmically with time; for large values of the piston velocity, they are locked in a very regular periodic profile. For all values of the piston velocity, one formula gives the speed of the shock front (speed of the leading soliton) as a function of the piston velocity. (3) As one moves through the *transition region* from the front to the rear of the shock wave, the local wave number increases to a value of π, the highest wave number which the discrete lattice can support. In this "binary" or "optical" mode, the displacement of adjacent particles is equal and opposite. This increase in the wave number is rather gradual for small values of the piston velocity, while it is very rapid (almost immediate) for large values of the piston velocity. Also, the lattice behind the shock front occupies a length which is foreshortened by the distance that the piston has traveled into the material. This compression introduces a local pressure

which must be taken into account in order to fit the shock profile to a soliton wave train. (4) At the *rear* of the shock near the piston, the lattice is compressed and is in the binary mode for all values of the piston velocity. For large values of the piston velocity u_p, the velocities of the particles near the piston relax to a finite-amplitude, steady oscillation about u_p as time increases. For small values of the piston velocity, these particles "thermalize" to zero temperature; that is, the amplitude of the velocity oscillations decays to zero as time increases according to a $t^{-1/2}$ decay law. The numerical experiments indicate a critical value of the piston velocity, above which the rear of the shock experiences steady, nonthermalized oscillations and below which it thermalizes. We establish the existence and exact value of this critical piston velocity by using the nonlinear transformation theory.

Because this paper is self-contained, it seems appropriate to list explicitly those results which we have not found in the literature, and hence are presumably new: (1) The use of the mathematics of the Toda lattice under time-independent boundary conditions (solitons, soliton wave trains, and the nonlinear transform) to analyze and empirically fit time-dependent shock waves on discrete chains, (2) the formula for fitting shock speed as a function of piston velocity for all values of this velocity, (3) the mathematical existence of a critical value for the piston speed (as established by using the nonlinear transform appropriate to shock boundary conditions), (4) the importance of the binary mode and the limitation of long-wavelength modes to the fronts of weak shock waves, and (5) the use of the spectral transform to measure numerically the soliton and soliton wave-train content of the shock profile.

We emphasize several points. (1) For most values of the piston speed, the shock profile is predominantly in the binary mode. Since, in this mode, the displacement of adjacent particles is equal and opposite, the lattice can be replaced by a two-particle lattice which is repeated periodically. This "binary approximation" is very easy to use. Its range of applicability is directly opposite to that of the "continuum" or "long-wavelength" approximation in which the lattice difference equations are replaced by partial differential equations. For shock waves on a lattice, this long-wavelength approximation is of limited use because of the predominance of the short-wavelength optical mode. In the text we discuss the validity of these various approximations as they apply to shock waves on the chain.

(2) We emphasize that we are discussing shock waves in conservative systems, and thus a conservative mechanism for the smoothing of shock waves. On a one-dimensional chain, dispersion causes the front to spread, while nonlinearity (if present) restrains this spreading. These two mechanisms (dispersion and nonlinearity) acting together produce solitons. The leading soliton defines the shock front, and the shock profile is a soliton wave train. This conservative mechanism for the smoothing of shock waves should be contrasted with the more familiar mechanism of (weak) dissipation. The two different mechanisms produce shock profiles with different structures and *shock fronts which move at different speeds as a function of the piston velocity*. This fact is discussed in some detail in the text, both with respect to shock waves on discrete chains and in continuum systems such as the Korteweg–de Vries (KdV) system.

(3) When describing basic physics, dissipation is not present. Dissipation is introduced when the full system is replaced by a small subsystem, which then interacts with its environment through a dissipative mechanism. For example, a shock wave in a three-dimensional system is approximated as one dimensional; in the process, degrees of freedom which are transverse to the shock direction are replaced by some form of weak dissipation. Our results apply only when such dissipation can be ignored.

The results which have just been summarized are established in Secs. V and VI. In Sec. V, we take analytical expressions for solitons and soliton wave trains and fit them to the shock profile, thereby interpreting the numerical observations in terms of fundamental nonlinear excitations. We also examine the validity of the binary and continuum approximations in different regions of the shock profile. In Sec. VI, we use two forms of the nonlinear transform to measure the actual nonlinear excitations in the shock profile. In Secs. II, III, and IV, we define the problem, fix our notation, and summarize some mathematical formulas.

II. DYNAMICS AND SHOCK-WAVE BOUNDARY CONDITIONS

In this section, the shock-wave problem is formulated with special attention given to (1) the meaning of two different boundary conditions that generate shock waves, (2) the significance of two different sets of units, and (3) the origin of an effective pressure in the interior of the shock wave. Consider a one-dimensional, monatomic chain of N particles, each of mass m, interacting with nearest neighbors only through a pairwise addi-

tive potential ϕ. The position of particle n at time t is denoted by $x_n(t)$, its velocity by $\dot{x}_n(t)$. The classical Hamiltonian H is given by

$$H=\sum_{n=1}^{N}\tfrac{1}{2}m\dot{x}_n^2(t)+\sum_{n=1}^{N}\phi(x_n-x_{n-1}), \tag{2.1}$$

from which the classical equations of motion are obtained

$$m\ddot{x}_n(t)=-\frac{\partial H}{\partial x_n}=\phi'(x_{n+1}-x_n)-\phi'(x_n-x_{n-1}). \tag{2.2}$$

In our shock-wave studies, *quiescent initial conditions* have been assumed; that is, the initial temperature and pressure are zero and particles $1\leq n\leq N$ are initially located motionless at their lattice sites:

$$\begin{aligned} x_n(0)&=na_0,\\ \dot{x}_n(0)&=0. \end{aligned} \tag{2.3}$$

The equilibrium lattice spacing (a_0 at zero pressure and temperature) is defined by

$$\phi'(a_0)=0.$$

Next we describe the two boundary conditions for generating shock waves. The simplest way to generate a shock wave in a one-dimensional chain is to impose *piston-shock* boundary conditions. The special particle $n=0$ is assumed to be infinitely massive, moving steadily at piston velocity u_p:

$$x_0(t)=u_pt. \tag{2.4}$$

As the piston particle approaches its neighbor ($n=1$), the two "collide," initiating a shock wave that moves out in front of the piston at shock velocity u_s.

In actual symmetric-impact shock-wave experiments, two flying plates approach each other at velocities $\pm u_p$ and collide, sending shock waves out from their interface at velocities $\pm u_s$. This experimental situation can be modeled by *shrinking-periodic boundary conditions* (PBC). Consider an N-particle lattice whose length L is forced to shrink at a constant rate,

$$L(t)=Na_0-2u_pt. \tag{2.5}$$

This shrinking generates two shock waves moving into the interior, one from each boundary. If this N-particle lattice is periodically repeated,

$$x_{n+N}(t)=x_n(t)+L(t), \tag{2.6}$$

then each interface (for example, between particles $n=N$ and $N+1$, or rather, its periodic image $n=1$) resembles the interface in the symmetric-impact experiment.

Because the shrinking-PBC shock-wave scheme is closer to the way real-world shock-wave experiments are performed, we prefer it to the piston scheme; the only significant differences observed in computer experiments are a quicker approach to the asymptotic shock-front shape and a slower approach to the long-time thermalization at the rear of the profile (near the "piston") for the PBC compared to piston boundary conditions. These differences arise from collisions of equal-mass particles as contrasted with collisions between a particle and an infinitely massive piston.

If the spatial derivative of the pair potential is expanded in a Taylor series, the equations of motion become

$$\begin{aligned} m\ddot{x}_n(t)=&\phi''(a_0)[(x_{n+1}-x_n-a_0)-(x_n-x_{n-1}-a_0)]+\tfrac{1}{2}\phi'''(a_0)[(x_{n+1}-x_n-a_0)^2-(x_n-x_{n-1}-a_0)^2]\\ &+\tfrac{1}{6}\phi''''(a_0)[(x_{n+1}-x_n-a_0)^3-(x_n-x_{n-1}-a_0)^3]+\cdots. \end{aligned} \tag{2.7}$$

This equation helps to motivate the following development, which we outline here briefly.

The *natural physical units* used are the mass m, the distance a_0 (equilibrium lattice spacing), the time ω_0^{-1}, where the fundamental harmonic frequency ω_0 is defined by $m\omega_0^2=\phi''(a_0)$; the velocity $c_0=a_0\omega_0$ (long-wavelength harmonic sound speed), $\nu=u_p/c_0$ (the scaled piston velocity), $\mu=u_s/c_0$ (the scaled shock velocity), and the energy mc_0^2. (2.8)

The *reduced variables and equations* are defined as follows: The time

$$s=\omega_0t, \tag{2.9}$$

the displacement

$$r_n(s)=\frac{x_n(t)-x_n(0)}{a_0}=\frac{x_n(t)}{a_0}-n, \tag{2.10}$$

the pair potential

$$\psi(r) = \frac{\phi(x)}{mc_0^2},$$

the cubic anharmonicity

$$\alpha_3 \equiv -\frac{a_0}{2}\frac{\phi'''(a_0)}{\phi''(a_0)},$$

the quartic anharmonicity

$$\alpha_4 \equiv \frac{a_0^2}{6}\frac{\phi'''(a_0)}{\phi''(a_0)},$$

and the equations of motion are

$$\ddot{r}_n(s) = \psi'(r_{n+1} - r_n) - \psi'(r_n - r_{n-1})$$
$$= r_{n+1} - 2r_n + r_{n-1} - \alpha_3[(r_{n+1} - r_n)^2 - (r_n - r_{n-1})^2] + \alpha_4[(r_{n+1} - r_n)^3 - (r_n - r_{n-1})^3] + \cdots . \quad (2.11)$$

The initial conditions are

$$r_n(0) = \dot{r}_n(0) = 0. \quad (2.12)$$

The boundary conditions are

$$r_0(s) = \nu s \quad \text{(piston)},$$
$$r_{n+N}(s) = r_n(s) - 2\nu s \quad \text{(PBC)}. \quad (2.13)$$

For our study, we have chosen a particular pair potential, the Toda pair potential,[3] which can be written with $\alpha \equiv \alpha_3$ as

$$\phi(x) = \frac{mc_0^2}{4\alpha^2}\left\{\exp\left[-2\alpha\left(\frac{x}{a_0} - 1\right)\right] + 2\alpha\left(\frac{x}{a_0} - 1\right) - 1\right\}, \quad (2.14)$$

or in reduced form,

$$\psi(r) = \frac{1}{4\alpha^2}[\exp(-2\alpha r) + 2\alpha r - 1]. \quad (2.15)$$

This potential smoothly interpolates between the "harmonic" and "hard-sphere" potentials as the anharmonicity parameter α runs from zero to infinity.

For mathematical convenience, a further scaling of the Toda equations can now be made; for the displacement let

$$q_n(s) = 2\alpha r_n(s), \quad (2.16)$$

with the momentum given by

$$p_n(s) = \dot{q}_n(s). \quad (2.17)$$

The *mathematical units and reduced equations* used in our analysis are the length $a_0/2\alpha$, the velocity $c_0/2\alpha$ (piston velocity, $2\alpha u_p/c_0 = 2\alpha\nu$), the energy $mc_0^2/4\alpha^2$, and the Toda potential

$$V(q) = \exp(-q) + q - 1. \quad (2.18)$$

The Hamiltonian is

$$h = \sum_{n=1}^{N} \tfrac{1}{2}p_n^2(s) + \sum_{n=1}^{N} [\exp(q_{n-1} - q_n) + q_n - q_{n-1} - 1]. \quad (2.19)$$

The equations of motion are

$$\dot{q}_n(s) = \dot{p}_n(s) = \exp(q_{n-1} - q_n) - \exp(q_n - q_{n+1}). \quad (2.20)$$

The initial conditions are

$$q_n(0) = p_n(0) = 0, \quad (2.21)$$

and the boundary conditions are

$$q_0(s) = 2\alpha\nu s \quad \text{(piston)},$$
$$q_{n+N}(s) = q_n(s) - 4\alpha\nu s \quad \text{(PBC)}. \quad (2.22)$$

[Equations (2.20), (2.21), and (2.22) in these units will be used in our analysis.]

Notice that, in these mathematical units, no parameters appear in the Toda potential nor in the equations of motion. The one parameter, the product $\alpha\nu$, appears only in the boundary conditions. Another set of units exists in which the unit of velocity is the piston velocity u_p and where the one parameter $\alpha\nu$ appears in the equations of motion, but not in the boundary conditions. Those units were used in the numerical computations. In both cases, however, it is clear that particle-velocity histories, as functions of time s or shock profiles as functions of space n, depend only on the product $\alpha\nu$, regardless of separate variations in α or ν. For example, the shock velocity $\mu = u_s/c_0$ is a function of the product $\alpha\nu$ only. This parametrization of profiles by $\alpha\nu$ is possible for any three-parameter (energy mc_0^2, length a_0, anharmonicity α) pair potential.

We close this section with a detailed discussion of the compression of the lattice caused by a shock wave. This compression is essential to the local description of the dynamics in the interior of a shock wave in a Toda chain, especially near the piston. Consider a *small chunk* of Toda lattice within the interior of the shock wave. This small lattice is moving at an average velocity equal to that of the piston u_p and with an average lattice spacing compressed to $a_\xi < a_0$. The physical origin of this compression is clear—the shock front and the piston particle move at different speeds. If the shock front, moving at speed u_s, reaches particle n at time t, then the compressed length

occupied by the n shocked particles is

$$na_\xi = (u_s - u_p)t. \tag{2.23}$$

Using $u_s t = na_0$ and the strain ξ defined by

$$\xi \equiv 1 - a_\xi/a_0, \tag{2.24}$$

we find from Eq. (2.23) that the compression strain due to the shock wave is

$$\xi = \frac{u_p}{u_s} = \frac{\nu}{\mu}, \tag{2.25}$$

where the second expression is in terms of the scaled speeds $\nu = u_p/c_0$ and $\mu = u_s/c_0$.

Next, we show there are two equivalent ways to incorporate this compression into a model of the small chunk of lattice, one through boundary conditions and the second through a time scaling. Suppose that lattice sites in a compressed chain are given by

$$x_n^{(\xi)} = na_\xi.$$

Displacements from these compressed lattice sites can then be expressed as

$$r_n^{(\xi)} = \frac{x_n - x_n^{(\xi)}}{a_0},$$

where the actual positions of the particles x_n are independent of the chosen lattice-site scheme. The relationship between displacements measured from uncompressed and compressed lattice sites is

$$r_n^{(0)} = r_n^{(\xi)} - n\xi,$$

or, in terms of the mathematical units,

$$q_n^{(0)} = q_n^{(\xi)} - 2n\alpha\xi. \tag{2.26}$$

The most natural expression of periodic boundary conditions for the small model lattice is given by the compressed lattice-site scheme,

$$q_{n+N}^{(\xi)} = q_n^{(\xi)}. \tag{2.27}$$

In the uncompressed lattice-site scheme, these boundary conditions become

$$q_{n+N}^{(0)} = q_n^{(0)} - 2N\alpha\xi = q_n^{(0)} + \mathfrak{L}, \tag{2.28}$$

where the lattice displacement $\mathfrak{L}$ (negative for positive compression) is

$$\mathfrak{L} = -2N\alpha\xi. \tag{2.29}$$

The equations of motion [Eq. (2.20)] for the small model lattice with *uncompressed* lattice sites are

$$\dot{p}_n^{(0)}(s) = \exp(q_{n-1}^{(0)} - q_n^{(0)}) - \exp(q_n^{(0)} - q_{n+1}^{(0)}),$$

subject to periodic boundary conditions [Eq. (2.28)]:

$$q_{n+N}^{(0)} = q_N^{(0)} + \mathfrak{L}.$$

Alternatively, the effect of compression can be put into the equations of motion by substitution of the relationship between displacements measured from uncompressed and compressed lattice sites [Eq. (2.26)]

$$\dot{p}_n^{(\xi)}(s) = \exp(q_{n-1}^{(\xi)} - q_n^{(\xi)} + 2\alpha\xi) - \exp(q_n^{(\xi)} - q_{n+1}^{(\xi)} + 2\alpha\xi).$$

We now note the fact that when time is scaled according to

$$\hat{s} = s\exp(\alpha\xi), \tag{2.30}$$

so that $d/ds = \exp(\alpha\xi)d/d\hat{s}$, the equations of motion for the small model lattice with *compressed* lattice sites become

$$\dot{p}_n^{(\xi)}(\hat{s}) = \exp(q_{n-1}^{(\xi)} - q_n^{(\xi)}) - \exp(q_n^{(\xi)} - q_{n+1}^{(\xi)}),$$

subject to periodic boundary conditions [Eq. (2.27)]

$$q_{n+N}^{(\xi)} = q_n^{(\xi)}.$$

This is *exactly* the same form as for the $\xi = 0$ case. Thus, the effects of compression can be taken into account in the Toda chain by putting the compressional amplitude $\alpha\xi$ either into the boundary conditions via Eq. (2.28) or into the equations of motion via the scaled time unit of Eq. (2.30), a feat made possible only for the exponential repulsive potential. We emphasize that, for a shock wave, conservation of mass gives for the compressional amplitude [see Eq. (2.25)]

$$\alpha\xi = \frac{\alpha\nu}{\mu}, \tag{2.31}$$

which is a function only of shock strength $\alpha\nu$. Finally, the rescaling of time by Eq. (2.30) is equivalent to rescaling the fundamental harmonic frequency:

$$\hat{\omega}_0 = \omega_0\exp(\alpha\xi). \tag{2.32}$$

This is an explicit statement of the quasiharmonic theory of lattice dynamics for the Toda, or exponential, lattice under compression.

III. SUMMARY OF NUMERICAL STUDIES

Shock waves in the Toda lattice have been studied by Holian and Straub[1] and by Straub, Holian, and Petschek[2] using the numerical method of molecular dynamics, namely, solving the equations of motion subject to shrinking-periodic boundary conditions for the Toda pair potential. These boundary conditions simulate the symme-

tric impact of two semi-infinite chains originally moving at $\pm u_p$, in that the periodic boundary behaves like the interface from which two shock waves emerge, traveling at $\pm u_s$. Figures 1–3 show the particle-velocity profiles, or time histories, of a sequence of particles down the initially quiescent chain, for three shock strengths: $\alpha v = 0$ (harmonic), $\alpha v = 0.525$ (weakly anharmonic), and $\alpha v = 52.5$ (strongly anharmonic, approaching the hard-rod, or one-dimensional hard-spheres limit), respectively. In Table I the salient features of these computer experiments are summarized. No significant qualitative differences in these observations are found if, instead of the Toda potential, Lennard-Jones (inverse-power) or Morse (exponential) potentials are used.

At the *front* of the shock, the leading pulse in the nonlinear cases approaches constant shape (amplitude and width) and speed, while in the linear case the pulse forever broadens due to dispersion. The oscillations in the transition region behind the front decay exponentially, but at qualitatively different rates in the linear and nonlinear cases; in the linear chain the exponential decay time, or shock thickness, grows like $t^{1/3}$ due to linear dispersion, while in the nonlinear chains, the shock thickness, where most of the elastic energy is stored, grows like t and is, therefore, a constant fraction of shocked material. The initial oscillatory frequency ω_1 is determined from the arrival times of the first and second peaks in the shock wave. For the linear lattice the peaks separate slowly with time

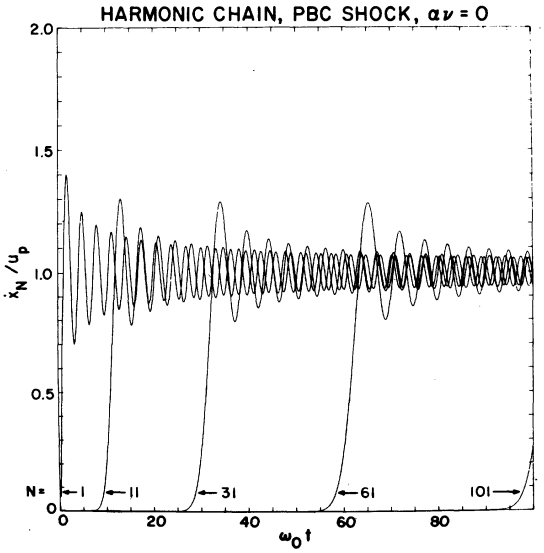

FIG. 1. Molecular-dynamics particle-velocity profiles (time histories) for a harmonic shock wave ($\alpha v = 0$) generated by shrinking-periodic boundary conditions.

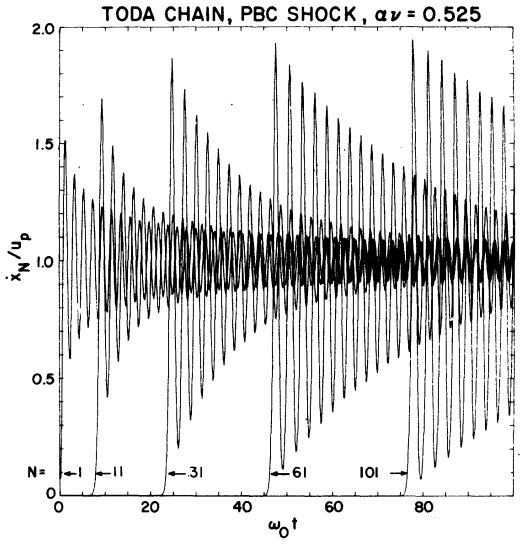

FIG. 2. Molecular-dynamics particle-velocity profiles for a weakly anharmonic shock wave ($\alpha v = 0.525$) generated by shrinking-periodic boundary conditions.

$s = \omega_0 t$ as the wave travels down the chain, so that $\omega_1/\omega_0 \sim n^{-1/3} \sim s^{-1/3}$. For a weakly nonlinear shock wave ($\alpha v = 0.02$), we have experimentally observed an even slower spreading with time, so that $\omega_1/\omega_0 \sim (\ln n)^{-1} \sim (\ln s)^{-1}$, confirming an earlier prediction based on analysis of Korteweg–deVries (KdV) shock waves.[4] For moderate-strength shock waves (e.g., $\alpha v \sim 0.5$), the temporal spreading is observed to be even slower than logarithmic, approaching the steady binary behavior of very strong shock waves ($\alpha v \gg 1$).

The oscillations long after the shock wave has

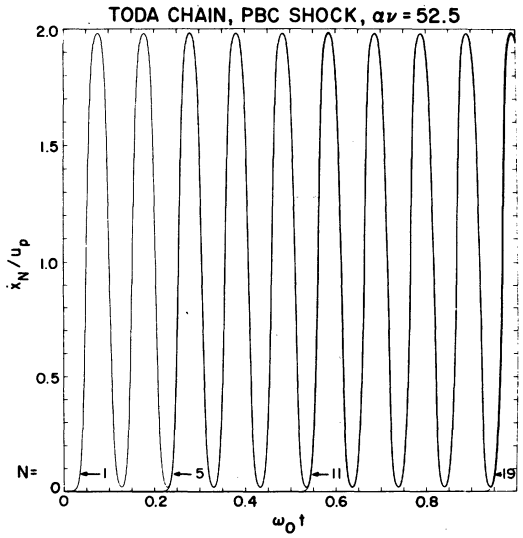

FIG. 3. Molecular-dynamics particle-velocity profiles for a strongly anharmonic shock wave ($\alpha v = 52.5$) generated by shrinking-periodic boundary conditions.

TABLE I. Summary of molecular dynamics experiments in one-dimensional, nearest-neighbor Toda chains.

Shock strengths	$\alpha\nu=0$ (see Fig. 1)	$0<\alpha\nu\ll 1$ (see Fig. 2)	$\alpha\nu\gg 1$ (see Fig. 3)
Initial pulse ($\omega_0 t\cong n/\mu, n\to\infty$)	Linear, dispersive	Soliton	Soliton
Amplitude, $\max(\dot{x}_n/u_p)$	1.3	2	2
Width, Δn (particles)	$\sim n^{1/3}$	$\sim(\alpha\nu)^{-1/2}$	~ 1
Speed, $\mu=u_s/c_0$	1 (harmonic)	$1+\frac{2}{3}\alpha\nu+\cdots$ (continuum, KdV)	$2\alpha\nu/\ln 4\alpha\nu$ (binary)
Initial oscillatory envelope	Exponential decay	Exponential decay	Weak exponential decay
Thickness, relaxation time	$\sim n^{1/3}$	$\sim n$	$\sim n$
Frequency, ω_1/ω_0	$\sim n^{-1/3}$	$\sim 1/\ln n$ (for $\alpha\nu<0.1$)	$2\pi\alpha\nu/\ln 4\alpha\nu$ (binary)
Final oscillations ($\omega_0 t\to\infty$)	Power-law decay	Power-law decay	No decay, steady oscillations
Amplitude, $\max(\dot{x}_n/u_p)-1$	$\sim(\omega_0 t)^{-1/2}$	$\sim(\omega_0 t-n/\mu)^{-1/2}$	$1-1/\alpha\nu$
Frequency, ω_∞/ω_0	2 (harmonic)	$2\exp(\alpha\nu/\mu)$ (quasiharmonic)	$2\pi\alpha\nu/\ln 4\alpha\nu$ $=\omega_1/\omega_0$ (binary)

passed, that is, at the *rear* of the profile near the piston, show a transition with shock strength $\alpha\nu$ from dispersive harmonic behavior at $\alpha\nu=0$ to hard-rod binary-collision soliton behavior at $\alpha\nu=\infty$. In the linear case shown in Fig. 1, the long-time-tail ($t^{-1/2}$) decay of a given particle's velocity begins at $t=0$ when the shock wave is initiated; in the nonlinear case shown in Fig. 2, the shock front is much sharper so that the decay starts at $\omega_0 t\cong n/\mu$, the arrival time of the shock wave at particle n. For $\alpha\nu<1$, the final amplitude of oscillation damps down to zero and the frequency ω_∞ is equal to the maximum allowed in the compressed chain by the quasiharmonic theory. For $\alpha\nu>1$, as shown clearly in Fig. 3, the final amplitude is nonzero and the frequency approaches that of binary collisions, which is higher than the infinitesimal-amplitude quasiharmonic frequencies. Careful analysis of the experimental time histories show that this transition occurs sharply at the critical value $\alpha\nu=1$.

Because of the importance of this critical transition, we discuss it in more detail. The long-time thermalization process was studied experimentally[2] by measuring the second-order cumulant of the velocity distribution, which becomes the thermodynamic temperature when the system reaches equilibrium:

$$T_n(t)=\frac{\langle(\dot{x}_n-\langle\dot{x}_n\rangle_t)^2\rangle_t}{u_p^2}. \tag{3.1}$$

Here the angular brackets indicate a time average over several collision times, or oscillatory periods, centered at time t:

$$\langle f\rangle_t=\frac{1}{\tau}\int_{t-\frac{1}{2}\tau}^{t+\frac{1}{2}\tau}dt' f(t'). \tag{3.2}$$

An approximate calculation of these time averages allows us to relate the function T_n to the amplitude A of the long-time oscillations in particle velocity. For such a calculation, it is convenient to choose some multiple of the long-time oscillatory period $2\pi/\omega_\infty$ for the time interval τ over which to average [Eq. (3.2)], and to treat the amplitude over this interval as essentially constant. For very large values of $\alpha\nu$ compared with unity, the wave form for a long-time oscillatory velocity is a square wave of amplitude $A(\infty)$. For small values of $\alpha\nu$ compared with unity, the wave form is sinusoidal with a slowly time-dependent amplitude $A(t)$. In these two limits, the second-order cumulant is then computed to be

$$T_n(t)\cong\begin{cases}\frac{1}{2}A^2(t), & \alpha\nu\ll 1\\ A^2(\infty), & \alpha\nu\gg 1.\end{cases} \tag{3.3}$$

The factor of $\frac{1}{2}$ in the small $\alpha\nu$ case is the result of the time average of $\sin^2\omega_\infty t$, while the factor of unity in the large $\alpha\nu$ case is due to the time average of a square wave.

A numerical experiment for a PBC shock wave at $\alpha\nu=1.05$ demonstrates the validity of this relationship between "temperature" and amplitude. The second-order cumulant was fit to high accuracy by the form

$$T_n(t)=\epsilon+\frac{B}{t-t_n}. \tag{3.4}$$

This fit was made for long times after the arrival time for the shock wave ($\omega_0 t_n=n/\mu$), namely, $200\lesssim\omega_0(t-t_n)\lesssim 1000$. The values $\epsilon=0.0011$ and $B=1.09$ were found. The final amplitude could not be observed directly, even at these long times; however, from observations of somewhat larger $\alpha\nu$ shocks, we have noticed that the final amplitude can be fit to the following simple function with virtually no error:

$$A(\infty)=\begin{cases}0, & \alpha\nu\lesssim 1\\ 1-\dfrac{1}{\alpha\nu}, & \alpha\nu>1.\end{cases} \tag{3.5}$$

For $\alpha\nu=1.05$, $A(\infty)=0.047$, and since the wave form is more nearly sinusoidal than square wave, the $\alpha\nu\ll 1$ form of Eq. (3.3) implies $\epsilon=T_n(\infty)=0.0011$. The consistency of these two measurements confirms our notions on the relationship of temperature to amplitude.

Furthermore, note from Eqs. (3.3)–(3.5), that the nature of the long-time behavior of $A(t)$ changes dramatically at $\alpha\nu=1$:

$$A(t)=\begin{cases}0+\left(\dfrac{2B}{t-t_n}\right)^{1/2}, & \alpha\nu<1\\ (2\epsilon)^{1/2}+\dfrac{B}{(2\epsilon)^{1/2}(t-t_n)}+\cdots, & \alpha\nu>1.\end{cases}$$

For shock waves below the critical length, the oscillatory amplitude goes to zero with a $t^{-1/2}$ long-time tail. Above the critical strength, the amplitude approaches a constant with a different long-time tail, namely, t^{-1}.

As shown in Ref. 2, thermalization or equilibration behind the shock front, requires that the velocity distribution be Maxwellian (Gaussian), in which case the fourth- and higher-order cumulants are zero. Following the same approach that led to Eq. (3.3), we may relate the oscillatory amplitude to the kurtosis, or fourth-order cumulant of the velocity distribution

$$C_n(t)=\frac{\langle(\dot{x}_n-\langle\dot{x}_n\rangle_t)^4\rangle_t}{u_p^4}-3T_n^2(t)$$

$$=\begin{cases}0, & \alpha\nu\ll 1\\ -2A^4(\infty), & \alpha\nu\gg 1.\end{cases} \tag{3.6}$$

Because the kurtosis deviates from zero in proportion to the square of the temperature, it is difficult to measure for $\alpha\nu\gtrsim 1$; nevertheless, for $\alpha\nu=3$, a significantly nonzero value of $C_n(\infty)=-0.11\pm 0.01$ was seen experimentally. We therefore conclude from our analysis that shock waves below the critical strength of $\alpha\nu=1$ thermalize to zero final temperature. On the other hand, shock waves above the critical strength reach a nonzero final temperature, but do not *thermalize*, since the velocity distribution is demonstrably non-Maxwellian.

The shrinking-PBC's are compared in Fig. 2 with the piston boundary conditions in Fig. 4 for $\alpha\nu=0.525$. Notice that in the PBC experiment, the shock front approaches its asymptotic form sooner and that the coefficient of the long-time oscillatory tail is much larger. In the piston experiment the infinitely massive piston particle does not pump up the leading soliton as fast and allows the shocked material to equilibrate more quickly than in the symmetric-impact PBC case.

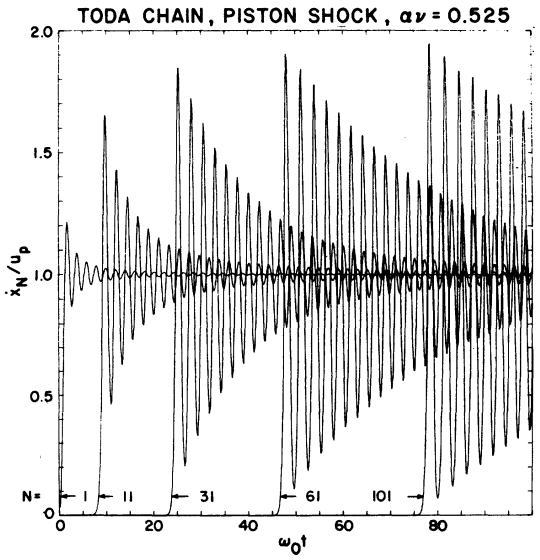

FIG. 4. Molecular-dynamics particle-velocity profiles for a weakly anharmonic shock wave ($\alpha\nu=0.525$) generated by piston boundary conditions (compare with Fig. 2).

IV. SPECIAL SIMPLIFIED MODELS

In this section, four simple models are presented which, under certain conditions, are applicable to various parts of the shock profile. For example, the leading pulse at the shock front ought to be describable by the first model considered, an isolated Toda soliton propagating into an undisturbed lattice, with width and speed fixed by the piston speed $2\alpha v$. Here mathematical formulas for this and the other simple models are presented. Where appropriate, derivations are given in the Appendices. (Data fitting, or comparison of the predictions of these models with experiment, is carried out in Sec. V.) The second model considered is the Toda periodic wave train, which should be able to describe the interior part of the shock wave. For weak shock waves, the leading edge ought to be well represented by the third model, the long-wavelength continuum limit. Two cases are discussed—the Korteweg–de Vries and continuum steady-wave solitons. For strong shock waves, the leading edge should be well suited to the fourth model, the binary-collision approximation, which should also be useful for describing the final long-time oscillatory state, regardless of shock strength.

A. Toda soliton

A soliton is a localized, steady, traveling-wave excitation in a nonlinear lattice. For the Toda chain, the analytical expression for the momentum of an isolated Toda soliton is

$$p_n(s) = 2\sinh^2\gamma\,\{\cosh\gamma + \cosh[2\gamma(n \mp \mu s) + \delta]\}^{-1}. \quad (4.1)$$

The Toda soliton is a two-parameter wave form with parameter γ fixing the amplitude, speed, and width, and with parameter δ merely centering the initial location of the excitation. The amplitude of the momentum pulse p_n is given by

$$A = 2(\cosh\gamma - 1). \quad (4.2)$$

Toda solitons can travel in either direction with constant supersonic speed

$$\mu = \frac{\sinh\gamma}{\gamma} = \frac{(A + \frac{1}{4}A^2)^{1/2}}{\ln[1 + \frac{1}{2}A + (A + \frac{1}{4}A^2)^{1/2}]}. \quad (4.3)$$

The full width at half maximum (FWHM) is

$$w = \frac{\cosh^{-1}(2 + \cosh\gamma)}{\gamma} = \frac{\ln[3 + \frac{1}{2}A + (8 + 3A + \frac{1}{4}A^2)^{1/2}]}{\ln[1 + \frac{1}{2}A + (A + \frac{1}{4}A^2)^{1/2}]}. \quad (4.4)$$

The higher the amplitude of a Toda soliton, the narrower it is and the faster it travels.

B. Toda periodic wave train

The periodic wave-train solution for the Toda lattice takes the analytical form

$$p_n(s; k, \omega) = \frac{d}{ds}\ln\frac{\Theta(z_n; q)}{\Theta(z_{n+1}; q)},$$

where k is the wave number (in units of $1/a_0$) and ω is the frequency (in units of ω_0) of the wave train. The phase is

$$z_n = \frac{kn - \omega s}{2\pi} + \delta,$$

and the nonlinear dispersion relation among k, ω, and q is

$$\omega^2 = -4\pi^2\left[\frac{d^2}{dz^2}\ln\Theta\left(z = \frac{k}{2\pi} - \tfrac{1}{2}\ln q; q\right)\right]^{-1},$$

with the θ function defined by the rapidly convergent infinite series for $0 \le q \le 1$:

$$\Theta(z; q) = \sum_{n=-\infty}^{\infty}(-1)^n q^{n^2}\exp(2\pi i n z).$$

This periodic traveling wave can be considered to be a three-parameter wave form parameterized by k, ω, and the phase-centering parameter δ, with the Θ-function amplitude parameter q determined by the dispersion relation. The phase speed of the wave train is

$$\mu = \omega/k.$$

Near the harmonic limit, the wave form is best written (using representations of the Θ function) as

$$p_n(s) = 4\omega\sum_{l=1}^{\infty}\frac{q^l}{1 - q^{2l}}\sin(\tfrac{1}{2}kl) \times \cos\left[\left(kn - \omega s + \frac{k}{2} + \delta\right)l\right], \quad (4.5)$$

and the dispersion relation is then given by

$$\omega = \left[\left(2\sin\frac{k}{2}\right)^{-2} - 2\sum_{l=1}^{\infty}\frac{lq^{2l}}{1 - q^{2l}}\cos(kl)\right]^{-1/2}. \quad (4.6)$$

As the amplitude parameter $q \to 0$, the harmonic (Fourier) solution for a linear lattice is recovered:

$$p_n(s) \to 4\omega q\sin\frac{k}{2}\cos\left(kn - \omega s + \frac{k}{2} + \delta\right)$$

and

$$\omega \to 2\sin\frac{k}{2}.$$

Near the soliton limit, an infinite-product representation of the Θ function is convenient. It gives

$$p_n(s) = 2\Omega \sinh\gamma \times \sum_{l=-\infty}^{\infty} \frac{1}{\{\cosh\gamma + \cosh[2\gamma(n-\mu s)+\gamma-4Ql]\}}, \tag{4.7}$$

and the dispersion relation is

$$\Omega = \left(Q^{-1} + \sum_{l=-\infty}^{\infty} \frac{1}{[\sinh(\gamma-2Ql)]^2}\right)^{-1/2}, \tag{4.8}$$

where the scaled parameters are

$$\Omega = \frac{Q}{\pi}\omega,$$

$$\gamma = \frac{Q}{\pi}k,$$

$$Q = -\tfrac{1}{2}\pi^2(\ln q)^{-1}.$$

The phase velocity is now written

$$\mu = \omega/k = \Omega/\gamma.$$

Notice that except for constants, the representation in Eq. (4.7) of the Toda periodic wave train is a sum of Toda solitons [see Eq. (4.1)], one centered at γ, and the rest translated by l periods from γ ($4Q$ is the wave-train period). If the period $4Q$ is allowed to go to infinity, keeping γ constant, thus isolating the solitons, the dispersion relation becomes

$$\Omega \to \sinh\gamma,$$

giving for the wave form

$$p_n(s) \to 2\sinh^2\gamma\{\cosh\gamma + \cosh[2\gamma(n-\mu s)+\gamma]\}^{-1},$$

which is the single Toda soliton.

For a wave train on a compressed lattice, the dispersion relation Eq. (4.8) becomes

$$\hat{\Omega} = \Omega\exp(\alpha\xi),$$

[compare with Eq. (4.32)]. The Toda dispersion relation is shown in Fig. 5 as frequency versus wave-number curves at constant amplitude parameter, for the uncompressed Toda chain. For $q < \frac{1}{2}$, the near-harmonic expression, Eq. (4.6), is computationally more quickly convergent; for $q > \frac{1}{2}$, the near-soliton form, Eq. (5.7) is faster.

C. Continuum approximation

The third mathematical model is the long-wavelength, or small-wave-number ($k \to 0$) limit, where excitations span several particles and the exact Toda equations can be replaced by a continuum approximation. In this approximation displacements form a continuum field in space n and time

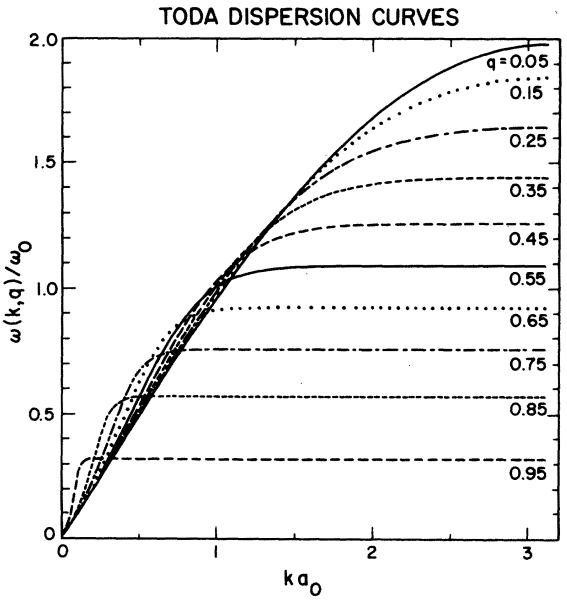

FIG. 5. Dispersion curves for the uncompressed Toda chain: frequency ω versus wave number k at constant amplitude parameter q ($q = 0$ at the harmonic limit, $q = 1$ at the soliton limit).

s:

$$q_n(s) \equiv q(n, s),$$

$$\dot{q}(n, s) \equiv \frac{\partial q(n, s)}{\partial s},$$

$$q'(n, s) \equiv \frac{\partial q(n, s)}{\partial n}.$$

The discrete (integer) Lagrangian coordinate labeling each mass point is now a continuous spatial variable n. The displacement field does not vary much from neighbor to neighbor, so that q can be expanded in a Taylor series:

$$q(n \pm 1, s) = q(n, s) \pm q'(n, s) + \tfrac{1}{2}q''(n, s) \pm \tfrac{1}{6}q'''(n, s) + \cdots.$$

The second-order, ordinary differential equations of motion [Eq. (2.7)], can then be written as a second-order, nonlinear, partial differential equation (retaining up to third degree in the displacement field and fourth order in spatial derivatives, i.e., quadratic anharmonicity and linear dispersion, respectively):

$$\ddot{q} = q'' + \tfrac{1}{12}q'''' - q'q'' + \tfrac{1}{2}q'^2q'' + \cdots. \tag{4.9}$$

In Appendix A, it is shown that by including only terms up to quadratic degree in the field q, the long-wave, moderate-amplitude, right-running solution to Eq. (4.9) satisfies the Korteweg–de Vries (KdV) equation

$$\dot{p} + p' + \tfrac{1}{24}p''' + \tfrac{1}{2}pp' = 0, \tag{4.10}$$

where the momentum field p is given by

$$p(n, s) \cong \dot{q}(n, s) \cong p_n(s).$$

The nonlinear KdV equation supports a localized, steady, traveling pulse, or KdV soliton[5]

$$p(n, s) = \gamma^2 \operatorname{sech}^2[\gamma(n - \mu s) + \delta], \tag{4.11}$$

where the amplitude is

$$A = \gamma^2, \tag{4.12}$$

the soliton speed is[5]

$$\mu = 1 + \tfrac{1}{6}\gamma^2 = 1 + \tfrac{1}{6}A, \tag{4.13}$$

and the FWHM is

$$w = \frac{\ln(3+\sqrt{8})}{\gamma} = \frac{\ln(3+\sqrt{8})}{A^{1/2}}. \tag{4.14}$$

(The wave number and frequency of an isolated soliton are zero; the centering parameter δ is arbitrary.)

It is shown in Appendix B that a more general continuum soliton than the KdV soliton is obtained by seeking a steady-wave solution to the continuum equation of motion [Eq. (4.9)]. The continuum soliton obeys the equation of motion of a pseudoparticle in the steady-wave time variable $\theta = s - n/\mu$:

$$\ddot{p}(\theta) = -\frac{\partial \Psi(p)}{\partial p}. \tag{4.15}$$

Here the pseudopotential, whose terms in powers of p correspond to terms in powers of q in the Toda chain Hamiltonian, is given by (including up to quartic anharmonicity)

$$\Psi(p) = \tfrac{1}{2}p^4 + 2\mu p^3 - 6\mu^2(\mu^2 - 1)p^2. \tag{4.16}$$

The speed of this continuum soliton as a function of amplitude A is

$$\mu = [1 + \tfrac{1}{3}(A/\mu) + \tfrac{1}{12}(A/\mu)^2]^{1/2}$$
$$= 1 + \tfrac{1}{6}A + O(A^3). \tag{4.17}$$

For small A, where only cubic anharmonicity is important, the full width at half maximum is

$$w = \frac{\ln(3+\sqrt{8})}{\sqrt{A}}. \tag{4.18}$$

Notice that the KdV results [Eqs. (4.13) and (4.14)] are recovered from a first-order analysis of the continuum soliton, and the continuum soliton is recovered by a long-wavelength approximation of the Toda soliton.

D. Binary-collision approximation

The fourth mathematical model applies to the highest-frequency oscillations that are allowed in the discrete chain of particles. These occur for the mode whose wavelength $\lambda = 2$ (i.e., $k = \pi$), so that the displacement of adjacent particles is equal and opposite. In this limit, the problem reduces to a periodic, two-particle (binary) system ($N = 2$), with periodic boundary conditions given by Eq. (2.27):

$$q_{n+2}(\hat{s}) = q_n(\hat{s}). \tag{4.19}$$

Here, for generality and convenience, the case of a compressed lattice has been incorporated into the scaled time $\hat{s}$ of Eq. (2.30). The equations of motion [Eq. (2.20)] are then

$$\begin{aligned} \ddot{q}_1(\hat{s}) &= \exp(q_0 - q_1) - \exp(q_1 - q_2) \\ &= -2\sinh(q_1 - q_2), \\ \ddot{q}_2(\hat{s}) &= \exp(q_1 - q_2) - \exp(q_2 - q_3) \\ &= 2\sinh(q_1 - q_2). \end{aligned} \tag{4.20}$$

In Appendix C, it is shown that the binary frequency, that is, the relative oscillation frequency of the two-particle system, as a function of amplitude is

$$\omega = \frac{\pi}{2}\exp(\alpha\xi)\left(\int_0^{q_{\max}} \frac{dq}{(\hat{A}^2 + 8 - 8\cosh q)^{1/2}}\right)^{-1}, \tag{4.21}$$

where

$$\hat{A} = A\exp(-\alpha\xi),$$

ξ is the compressive strain, and

$$q_{\max} = \ln[1 + \tfrac{1}{8}\hat{A}^2 + \tfrac{1}{2}\hat{A}(1 + \tfrac{1}{16}\hat{A}^2)^{1/2}].$$

The speed of the binary wave train ($k = \pi$) is then

$$\mu = \omega/k = \omega/\pi,$$

and the FWHM is one particle

$$w = 1.$$

For small A, where only cubic anharmonicity is important, the frequency ω (in units of ω_0) reduces identically to the highest-allowed quasiharmonic frequency

$$\omega = 2\exp(\alpha\xi).$$

In other words, at least quartic anharmonicity is required in a truncated approximation to the Toda pair potential before there is any detectable deviation from the quasiharmonic theory. (See Appendix C for details.)

For large A, the binary-collision frequency becomes

$$\omega = \frac{\pi}{4}\frac{A}{\ln A - \alpha\xi}. \tag{4.22}$$

V. COMPARISON OF SIMPLE MODELS WITH EXPERIMENT

A. Toda soliton

In numerical experiments reported in Ref. 2, it was observed that a shock wave in the Toda lattice appears to behave very much like a succession of solitons, regardless of shock strength. If two shock waves are run toward each other *and the driving support suddenly removed,* that is, the pistons are stopped, the wave trains collide, with their peaks passing through each other essentially unchanged. Moreover, the peaks, which move with speeds in proportion to their amplitudes, spread out in time.

We now show that the leading edge of the shock front, the initial pulse, is indeed an isolated Toda soliton. As the pulse travels away from the piston, or shrinking-periodic boundary, its amplitude, as measured in the numerical experiments, approaches the hard-rod limit (see Ref. 4 for the KdV result)

$$\lim_{n\to\infty} \max \dot{x}_n(t) = 2u_p ; \tag{5.1}$$

consequently, the amplitude to be used in the formulas (4.1)–(4.4) for the Toda soliton is (in mathematical units)

$$A = 4\alpha v . \tag{5.2}$$

If the shock front is an isolated Toda soliton, its speed and width will be given as a function of αv by Eqs. (4.3) and (4.4):

$$\mu = \frac{(A+\frac{1}{4}A^2)^{1/2}}{\ln[1+\frac{1}{2}A+(A+\frac{1}{4}A^2)^{1/2}]} = \frac{[4\alpha v+4(\alpha v)^2]^{1/2}}{\ln\{1+2\alpha v+[4\alpha v+4(\alpha v)^2]^{1/2}\}} , \tag{5.3}$$

$$w = \frac{\ln[3+\frac{1}{2}A+(8+3A+\frac{1}{4}A^2)^{1/2}]}{\ln[1+\frac{1}{2}A+(A+\frac{1}{4}A^2)^{1/2}]} = \frac{\ln\{3+2\alpha v+[8+12\alpha v+4(\alpha v)^2]^{1/2}\}}{\ln\{1+2\alpha v+[4\alpha v+4(\alpha v)^2]^{1/2}\}} . \tag{5.4}$$

Over the *full* range of amplitude, the above asymptotic fitting of $A = 4\alpha v$ for the Toda soliton *matches* experimental observations of the leading pulses to within the accuracy of the molecular-dynamics experiments. Next, we ask over what range of αv are the continuum and binary approximations valid?

For small amplitude, the speed of the Toda soliton as given by Eq. (5.3) reduces to the continuum expression[4,5]

$$\mu = 1+\tfrac{1}{6}A+\cdots = 1+\tfrac{2}{3}\alpha v+\cdots , \tag{5.5}$$

while the width given by Eq. (5.4) becomes

$$w = \frac{\ln(3+\sqrt{8})}{\sqrt{A}} = \frac{\ln(3+\sqrt{8})}{(4\alpha v)^{1/2}} . \tag{5.6}$$

Comparison of these continuum expressions with numerical experiments shows that the continuum soliton is sufficient to describe the shock front for values of αv in the range $0 < \alpha v < 0.5$.

For large amplitude, the speed of the Toda soliton becomes

$$\mu = \frac{A}{2\ln A} = \frac{2\alpha v}{\ln 4\alpha v} , \tag{5.7}$$

while the width becomes

$$w = 1 .$$

These large-amplitude approximations of the Toda soliton agree with the binary approximation; however, the verification of the equivalence is slightly more subtle than the verification of the equivalence of the small-amplitude approximation with the continuum theories. It begins with the observation that the entire large-amplitude shock wave, all the way from the shock front to the piston, is a wave train of hard-rodlike Toda solitons in the binary mode. To obtain Eq. (5.7) from the binary approximation, first note that this train is under compression, which may be estimated using the speed of the shock front:

$$\alpha\xi = \frac{\alpha v}{\mu} = \frac{A}{4\mu} = \tfrac{1}{2}\ln A . \tag{5.8}$$

From Eq. (4.22), the binary collision frequency is

$$\omega = \frac{\pi A}{2\ln A} , \tag{5.9}$$

which gives the binary wave-train speed

$$\mu = \frac{\omega}{\pi} = \frac{A}{2\ln A} . \tag{5.10}$$

This binary result agrees with the speed of the large-amplitude Toda soliton Eq. (5.7) and comparison with numerical experiment shows the binary approximation is accurate for $\alpha v > 5$.

B. Continuum approximation

For weak shock waves, where $\alpha v < 0.5$, the KdV and continuum solitons are limiting forms of the Toda soliton, which provides a quantitative description of the leading edge of shock waves of all strengths in the Toda lattice. For the discrete cubic and quartic chains, where the pair potential has been truncated to include up to cubic and quartic anharmonicity, respectively, the con-

tinuum soliton gives a quantitative prediction of the shock speed for all shock strengths [see Eq. (5.17) for the Toda quartic case; the cubic result is obtained by dropping the term in $(A/\mu)^2$].

Analysis[3] of KdV shock waves yields the prediction that the first and second soliton peaks separate logarithmically in time, as the second-pulse amplitude asymptotically approaches that of the first pulse $A=4\alpha\nu$. We have confirmed this prediction for a very weak shock wave in the Toda chain, namely, $\alpha\nu=0.02$. The cube-root-of-time spreading seen in the linear chain was clearly not indicated in this weakly nonlinear case. However, at $\alpha\nu=0.105$, the spreading is even slower than logarithmic; by $\alpha\nu=0.525$, constant asymptotic separation appears to be likely. Certainly, in the hard-rod limit, the asymptotic separation is virtually instantaneous, so a transition is to be expected.

As is shown in Appendix B, the continuum equations of motion will support a steady, isolated pulse (continuum soliton), but will *not* support a steady solution in which the final particle velocity is equal to the piston velocity. We emphasize once again that such a *steady* shock profile is appropriate only in a dissipative system and not for a conservative one-dimensional chain. If that fact is nevertheless ignored, resulting analysis predicts an initial maximum particle velocity of $\frac{3}{2}u_p$, rather than the observed value $2u_p$, as well as a shock speed of $\mu=1+\frac{1}{2}\alpha\nu$, rather than the observed $\mu=1+\frac{2}{3}\alpha\nu$.

C. The Toda periodic wave train

To interpret the leading edge of the shock wave as a Toda soliton, it was not necessary to introduce a correction for pressure or compression since the leading edge sees no pressure. The interior of the shock wave, on the other hand, is under an effective pressure and should be described by a slowly varying Toda wave train. This description has not proved to be a very quantitative tool, largely because of uncertainty in the values of the local compression. In Sec. II, we estimate the local compression by its global average $\alpha\xi=\alpha\nu/\mu$. The Toda dispersion relation can be used to predict the temporal frequency of the wave train in terms of amplitude, speed, and compression. *Near the wave front*, we use the amplitude $A=4\alpha\nu$ as found in numerical experiments, the speed $\mu(A)$ discussed in the last section, and the average compression $\alpha\xi=A/4\mu$. The prediction of temporal frequency which results is better than that obtained by using no compression, but is still not very quantitative. The average estimate of pressure is too crude. For wave numbers near π, the Toda wave train is equivalent to the periodic train in the binary approximation, which is taken up next.

D. Binary-collision approximation

For the long-time oscillatory tail in the discrete lattice, the binary-collision approximation is appropriate for all shock strengths because the wave number is always π. Numerical experiments show that the long-time oscillatory tail has two amplitude regimes: the quasiharmonic regime

$$A=0, \quad 0<\alpha\nu<1 \tag{5.11}$$

and the hard-rod regime

$$A=4\alpha\nu-4, \quad \alpha\nu\geq 1. \tag{5.12}$$

Using the binary-collision approximation of Sec. IV D, we compute the frequency ω_∞ in terms of the amplitude A, the shock speed μ, and the average compression $\alpha\xi=\alpha\nu/\mu$. The agreement with experiment is fairly good; for $\alpha\nu$ near 0, it is almost exact, as it is for large $\alpha\nu$. As a function of $\alpha\nu$, the error in the binary prediction peaks at $\alpha\nu\sim 1$. There ω_∞ is underestimated by around 10%. This inaccuracy is due, once again, to an incorrect estimate of the local compression, which is higher near the piston than the average compression predicted from the speed of the leading soliton. The enhancement of compression near the piston arises from the nonsteady nature of shock waves in nonlinear, nondissipative, one-dimensional chains, where the shock thickness grows linearly with time. In other words, the region of thermal agitation behind the shock front is a constant fraction of the shocked material. Since the local compression is only slowly building up in this region, the final value near the piston will be larger if the fractional shock thick-

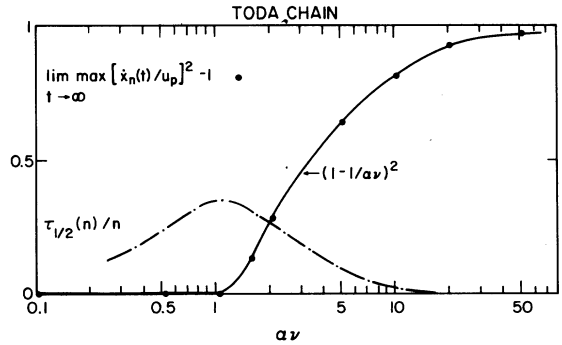

FIG. 6. Final square amplitude of the long-time oscillatory tail (molecular-dynamics results ●), $\lim_{t\to\infty}\max[\dot{x}_n(t)/u_p]^2-1$, which is zero for $\alpha\nu<1$ and $(1-1/\alpha\nu)^2$ for $\alpha\nu\geq 1$ (solid line ——), fractional shock thickness (thermal relaxation time) $\tau_{1/2}(n)/n$ (dash-dot line —·—). The shock strength in the Toda chain is $\alpha\nu$ (α = cubic anharmonicity, ν = piston velocity).

ness is also. As shown in Fig. 6, the fractional shock thickness as well as the increase in local compression near the piston is most pronounced near $\alpha v \sim 1$. A slight enhancement in $\alpha\xi$ near the piston boosts the calculated ω_∞, and brings the binary approximation into agreement with experiment.

Finally, it is clear from the numerical experiments that the break in the dynamics of the Toda lattice under shock compression, which occurs at the critical value $\alpha v = 1$, is a transition from the infinitesimal-amplitude harmonic (or quasi-harmonic, for $0 < \alpha v < 1$) behavior in the long-time oscillatory tail to finite-amplitude hard-rod ($\alpha v > 1$) behavior. (It is interesting to note that the discrete *quartic* chain also supports finite-amplitude long-time excitations of this binary mode, while the discrete *cubic* chain sinks into harmonic behavior. Of course, the αv criticality for the quartic chain occurs at a somewhat different value than $\alpha v = 1$, the full Toda chain criticality.)

VI. MEASUREMENTS USING THE SPECTRAL TRANSFORM

A. General remarks about the spectral transform

In this section we use a mathematical tool called the "inverse spectral transform" to measure the nonlinear excitations which are present in the shock profile. Two different versions of this transform are used, one to describe global properties of the shock wave and the second to measure its local structure. The first version (Sec. VI B) precisely identifies a threshold value for the piston speed, below which numerical experiments show that the lattice behind the shock wave thermalizes. The second version (Sec. VI C) of the transform provides a description of the local structure of the shock which is an alternative to the description of the shock profile as a function of the particle position n. The second version of the transform measures the soliton content of the shock front and the wave-train content of the excitation in the interior of the shock wave. In particular, the second version confirms a connection between the threshold for thermalization and finite-amplitude nonlinear binary oscillations of the lattice.

The spectral transform changes variables from (q_n, p_n) to new collective coordinates, in terms of which the Toda equations (under appropriate boundary conditions) are exactly solvable analytically. We call these new variables "nonlinear normal modes for the Toda lattice." Typically, these nonlinear modes belong to two classes—localized excitations (solitons) and dispersive radiation (soliton wave trains).

The nonlinear modes can be coordinated by action-angle variables, in terms of which the Toda equations (under appropriate boundary conditions) are trivial:

$$(q_n, p_n) \to (J_n, \theta_n),$$
$$\dot{J}_n = 0,$$
$$\dot{\theta}_n = \omega_n(J).$$

We will not describe the full transformation from (q_n, p_n) to (J_n, θ_n); rather, we emphasize one of its most important properties. While the complete transform is complicated, it is very easy at any fixed time s to compute numerically and to display graphically, the qualitative information contained in the *action variables*. In principle, these action variables (1) count the degrees of freedom which are excited in the shock profile, and classify them as solitons or radiation, (2) measure the speeds of the excited solitons, and (3) measure the frequencies, the wave numbers, and the amplitudes of the radiation wave trains which are present in the shock wave.

The spectral transform has been developed for phase configurations (q_n, p_n) under the following three types of boundary conditions:

Infinite, vanishing $(q_n, p_n) \to (0, 0)$ as $n \to \pm\infty$,

Infinite, shock $(q_n, p_n) \to \begin{cases} (2\alpha v s, 2\alpha v) & \text{as } n \to -\infty \\ (-2\alpha v s, -2\alpha v) & \text{as } n \to +\infty \end{cases}$,

Periodic $(q_{n+N}, p_{n+N}) = (q_n + \mathcal{L}, p_n)$.

Under each boundary condition, the transform begins with the second-order linear difference operator L,

$$(Lu)_n = a_{n-1}u_{n-1} + a_n u_{n+1} + b_n u_n. \tag{6.1}$$

Here the coefficients (a_n, b_n) are given in terms of the phase point (q_n, p_n) by

$$a_n \equiv \tfrac{1}{2}\exp\left(\frac{q_{n-1} - q_n}{2}\right),$$
$$b_n = -\tfrac{1}{2}p_{n-1}, \tag{6.2}$$

and these coefficients inherit the boundary conditions of the phase configuration.

As the coefficients flow in time according to the Toda equation (under the appropriate boundary conditions), certain spectral properties such as the eigenvalues of the operator L remain unchanged. The action variables are defined in terms of these spectral quantities. These spectral properties of L are, in turn, easy to compute and to display graphically. [To obtain some in-

tuition about the operator L and its spectral properties, set $a_n = \frac{1}{2}$ and $b_n = -1 - V_n$:

$$(Lu)_n = \tfrac{1}{2}(u_{n+1} - 2u_n + u_{n-1}) - V_n$$
$$\simeq \frac{1}{2}\frac{d^2}{dx^2} - V(x).$$

Spectral properties of the difference operator L are quite analogous to those of the Schrödinger operator in quantum mechanics.]

The spectral transform under infinite, vanishing boundary conditions and under periodic boundary conditions has been known for several years.[6-11] We will assume the reader is aware of this material. In particular, we will not repeat the tutorial material of Ref. 11, which is used extensively in Sec. VIC.

B. Spectral transform under shock boundary conditions

Under shock boundary conditions, the spectral transform is currently being developed.[12] In this section, we describe the transform under shock boundary conditions only to the extent needed in order to display a critical value in the shock strength (that is, in the piston speed). This critical value can be obtained directly from a spectral transform of the initial conditions.

Consider a shock wave initialized by the step initial conditions (at time $s=0$)

$$(q_n, p_n) = \begin{cases} (0, 2\alpha\nu), & n < 0 \\ (0, -2\alpha\nu), & n \geq 0. \end{cases}$$

Equivalently, in the (a_n, b_n) coordinates, Eq. (6.2) at time $s=0$,

$$(a_n, b_n) = \begin{cases} (\tfrac{1}{2}, -\alpha\nu), & n < -1 \\ (\tfrac{1}{2}, \alpha\nu), & n \geq -1. \end{cases}$$

The eigenvalue problem for the operator L,

$$(Lu)_n = a_{n-1}u_{n-1} + a_n u_{n+1} + b_n u_n = \lambda u_n, \qquad (6.3)$$

takes the initial form

$$\tfrac{1}{2}u_{n-1} + \tfrac{1}{2}u_{n+1} = \begin{cases} (\lambda + \alpha\nu)u_n, & n < -1 \\ (\lambda - \alpha\nu)u_n, & n \geq -1. \end{cases}$$

Since the spectrum of the operator L is invariant under Toda dynamics, it is sufficient to calculate the spectrum at time zero ($s=0$). The results of this calculation (see Appendix D) are summarized in the following *fact*: The spectrum of $L(s)$ consists in the union of two intervals

$$\lambda \in ([-1 - \alpha\nu, 1 - \alpha\nu] \cup [-1 + \alpha\nu, 1 + \alpha\nu]).$$

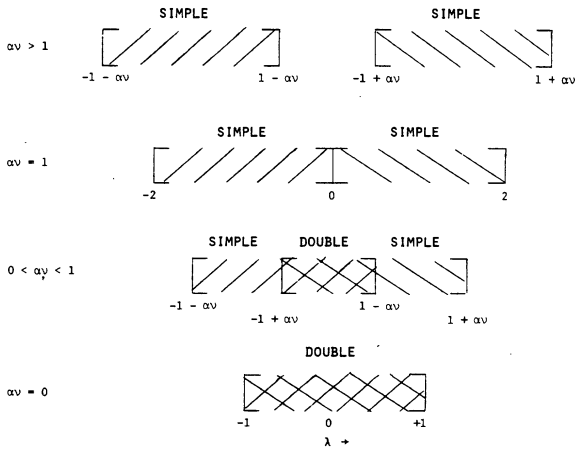

FIG. 7. Multiplicity of the spectrum of L (eigenvalue λ) as a function of shock strength $\alpha\nu$. Note the emergence of double spectrum for $\alpha\nu$ below the critical value of unity.

For λ in the intersection of these intervals, the spectrum is double; otherwise, it is simple. These spectral intervals are displayed in Fig. 7.

The key feature here is the multiplicity in the spectrum. Recall that a point λ is said to be in the spectrum of L if, for the value of λ, there exists an eigenfunction $u_n(\lambda)$ which is bounded for all n. If only one bounded eigenfunction exists, λ is called *simple*; if two linearly independent bounded eigenfunctions exist, λ is called *double*. Here, the spectrum of L lies in the union of two intervals; in their intersection it is double, elsewhere simple.

First, consider the case of a large amplitude shock wave with $\alpha\nu > 1$. As is clear from Fig. 7, the intersection $[-1 - \alpha\nu, 1 - \alpha\nu] \cap [-1 + \alpha\nu, 1 + \alpha\nu]$ is empty. The spectral intervals are disjoint; the entire spectrum is simple.

As the shock strength decreases to and below 1, the intervals overlap. The spectrum consists of two intervals of simple spectrum, with an interval of double spectrum in between.

We emphasize that $\alpha\nu = 1$ is a *critical* value. For shock strengths $\alpha\nu$ above 1, the spectrum is simple and lies in two disjoint intervals. For $\alpha\nu$ below 1, the spectrum lies in one interval; the interior of this interval consists in double spectrum, while the two exterior ends consist in simple spectrum. At precisely this value of piston speed, the criticality in the long-time behavior of the region behind the shock was observed in the numerical experiments. As yet, this physical effect (as described in Secs. III and V) has not been deduced directly from the scattering transform, but most certainly the change in the multiplicity of the spectrum at $\alpha\nu = 1$ is the key.

C. Spectral measurements of the local structure of the shock wave

From the empirical fits of Sec. V, it seems clear that the Toda shock wave is smoothed by Toda wave trains. Using the spectral transform under periodic boundary conditions, we can measure from the data the characteristics of such wave trains. In this section we take a chunk of lattice from the shock profile and measure its spectral content using the periodic spectral transform. From these measurements, we infer the local structure of the shock wave, and we show that these measurements agree with the empirical fitting to basic Toda excitations as described in Sec. V. In addition, we directly measure the local compression, the quantity which was missing in Sec. V.

Practical procedures for using the spectral transform under periodic boundary conditions to measure nonlinear modes have been described in detail in Ref. 11. We will not repeat that material here; rather, we emphasize an aspect of the spectral content of the shock profile which differs from the examples described in Ref. 11.

Consider a periodically repeated N-particle Toda lattice whose displacement is $\mathfrak{L}$ [Eq. (2.29)]:

$$q_{n+N} = q_n + \mathfrak{L}\,,$$

$$p_{n+N} = p_n\,.$$

Under these boundary conditions, a_n and b_n are strictly periodic of period N, and the second-order difference operator L is equivalent to the $N \times N$ matrix:

$$L = \begin{pmatrix} b_1 & a_1 & 0 & 0 & & & 0 & a_N \\ a_1 & b_2 & a_2 & 0 & & & & \\ 0 & a_2 & b_3 & a_3 & & & & \\ 0 & 0 & a_3 & b_4 & a_4 & & & 0 \\ 0 & & & & & & & \\ \vdots & & & & & & & \\ 0 & & & & & a_{N-2} & b_{N-1} & a_{N-1} \\ a_N & 0 & & & & 0 & a_{N-1} & b_N \end{pmatrix}. \tag{6.4}$$

As $a_n(s)$, $b_n(s)$ change in time s according to *periodic* Toda dynamics, the eigenvalues $\{\lambda_n\}$ of the matrix L remain unchanged, and provide N constants of motion for the Toda lattice. For example, the total momentum and total energy of the lattice are given in terms of these eigenvalues by the simple formulas

$$NP = \sum_{n=1}^{N} p_n = -2\,\mathrm{tr}L = -2\sum_{n=1}^{N} \lambda_n\,,$$

$$h = \sum_{n=1}^{N} \tfrac{1}{2}p_n^2 + V(q_n - q_{n-1}) \tag{6.5}$$

$$= 2\,\mathrm{tr}L^2 = 2\sum_{n=1}^{N} \lambda_n^2\,.$$

Instead of computing the eigenvalues $\{\lambda_n\}$ directly, we consider a polynomial $\Delta(\lambda)$ which is fixed by the eigenvalues and the lattice displacement $\mathfrak{L}$:

$$\Delta(\lambda) \equiv A\det(\lambda I - L) + 2$$

$$= A\prod_n (\lambda - \lambda_n) + 2\,. \tag{6.6}$$

Here the leading coefficient A is given in terms of $\mathfrak{L}$ by

$$A^{-1} = \prod_1^N a_n = (\tfrac{1}{2})^N \exp[-\tfrac{1}{2}(q_N - q_0)]$$

$$= (\tfrac{1}{2})^N \exp(-\tfrac{1}{2}\mathfrak{L})\,. \tag{6.7}$$

It is very easy, given the phase point (q_n, p_n), to compute numerically the polynomial $\Delta(\lambda)$ since the matrix L is (essentially) tridiagonal. As described in Ref. 11, the types of nonlinear modes which are initialized by the configuration (q_n, p_n), together with their physical characteristics, can be inferred directly from a graph of $\Delta(\lambda)$ vs λ.

For clarity, we emphasize that the region behind the shock wave is *not* a periodic Toda lattice; rather, it seems to behave locally as a slowly modulating Toda wave train. To quantify this observation, we take at time s, a chunk of lattice which consists of N masses behind the shock front and construct a model by periodically repeating this chunk of lattice. The discriminant $\Delta(\lambda)$ will directly measure the exact nonlinear mode content of this model; hence, it will indirectly measure the wave train which is smoothing the shock wave.

If the periodic model is allowed to flow in time under strictly periodic Toda dynamics, $\Delta(\lambda)$ will not change. However, if a second model is constructed for the chunk of lattice at time $s_1 > s$, $\Delta(\lambda, s_1) \neq \Delta(\lambda, s)$. In fact, the change in $\Delta(\lambda)$ will measure the modulations in the Toda wave train which is smoothing the shock wave. We repeat: The shock wave is not smoothed by an exact, periodic Toda wave train, but by a slowly modulating wave train. Temporal changes in $\Delta(\lambda)$ will measure these modulations.

First, consider the shock profile shown in Fig. 8. This profile was initiated by the piston moving at speed $\alpha v = 52.5$. The profile is pictured at time

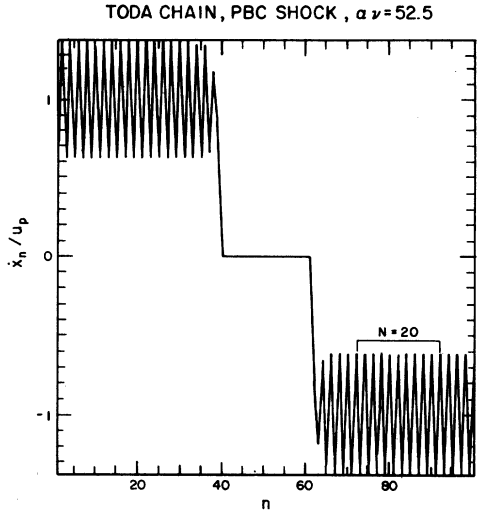

FIG. 8. Shock-wave profile of particle velocity $\dot{x}_n/u_p$ vs particle number n at $\omega_0 t=2$ for PBC shock of strength $\alpha\nu=52.5$. The discriminant in Fig. 9 was calculated for the segment of lattice in the interior of the profile marked by the box, $N=20$ particles wide.

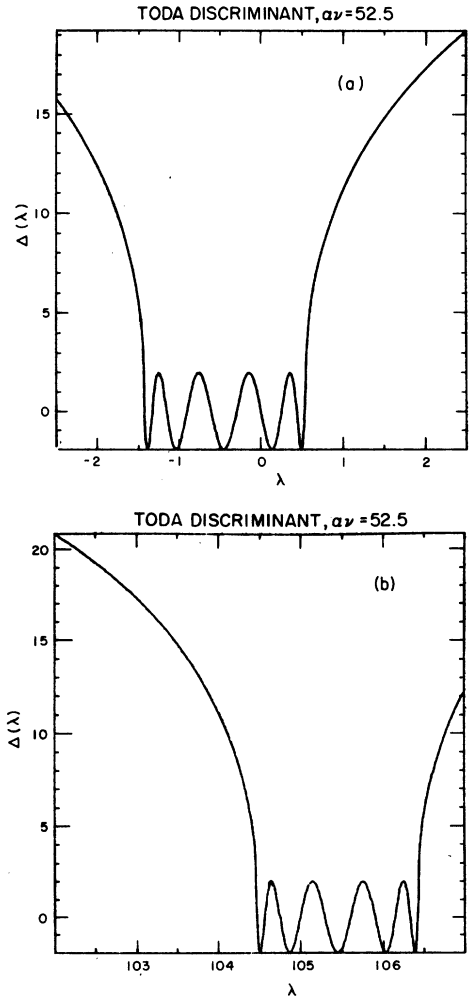

FIG. 9. Discriminant $\Delta(\lambda)$ for a Toda-chain shock wave $\alpha\nu=52.5$ at $\omega_0 t=2$ (see Fig. 8): (a) λ near 0; (b) λ near $2\alpha\nu$. (When $|\Delta|>2$, a logarithmic scale is used.)

$s=2$, at which time the shock front is located 39 particles from the piston. Figure 9 shows the discriminant $\Delta(\lambda)$ for a chunk of this profile, which is 20-particles wide, located near the rear of the shock profile. This chunk of the shock wave is shown by the box in Fig. 8.

Using the rules of Ref. 11, we interpret this measured discriminant. It shows two intervals of spectrum, located at $\lambda\in[-0.5,1.5]$ at $\lambda\in[104.5,106.5]$, separated by a large gap in the spectrum. Since all extrema are tangent to $\pm 2\,[\Delta(\lambda_{\rm ext})=\pm 2]$ except for the central peak, only one degree of freedom is excited in this region of the shock profile. This single degree of freedom is the highest wave-number (binary) mode.

A discriminant with this particular structure was not analyzed in Ref. 11; we do so here. This measured discriminant can be interpreted analytically using the binary approximation (Sec. IV D). First, we model the shock profile as a periodic repetition of a chunk of lattice which is two particles wide; that is, we model the shock wave as a "period-2" Toda lattice whose total displacement is $\mathfrak{L}=-4\alpha\xi$:

$$\ddot{q}_n=\exp(q_{n-1}-q_n)-\exp(q_n-q_{n+1}),\qquad q_{n+2}=q_n+\mathfrak{L}\,. \tag{6.8}$$

This effective two-body problem can be quickly integrated (see Appendix E):

$$Q(s)=Q(0)+Ps,\qquad \tfrac{1}{2}p^2+4\exp(-\tfrac{1}{2}\mathfrak{L})\cosh(q+\tfrac{1}{2}\mathfrak{L})=h. \tag{6.9}$$

Here, the center of mass and relative coordinates are given by $Q\equiv\frac{1}{2}(q_1+q_2)$, $q\equiv q_1-q_2$, and the two-body trajectory is parametrized by the length $\mathfrak{L}$, the center-of-mass momentum P, and the relative energy h.

In Appendix E, we explicitly calculate the discriminant $\Delta(\lambda)$, a quadratic in λ, for the two-body Toda lattice

$$\Delta(\lambda;P,\mathfrak{L},h)=4\exp[(\tfrac{1}{2}\mathfrak{L})(\lambda+\tfrac{1}{2}P)^2-\tfrac{1}{8}h]. \tag{6.10}$$

Notice that the binary discriminant is centered at $-\frac{1}{2}P$, its two intervals of spectrum are centered by h, and the width of these spectral intervals is fixed by $\mathfrak{L}$. To compare this two-body

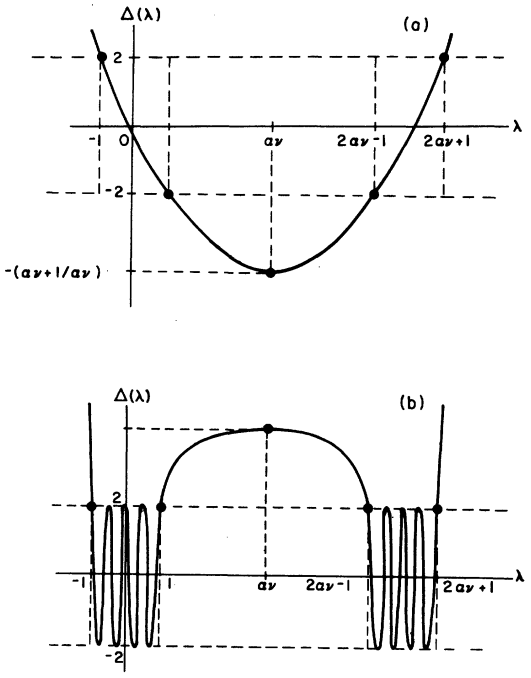

FIG. 10. (a) Binary (two-particle) discriminant $\Delta(\lambda)$ vs eigenvalue λ for a strong shock wave $\alpha\nu > 1$. (b) Discriminant $\Delta(\lambda)$ for 16-particle segment made up of eight two-particle periodically repeated units; same shock strength $\alpha\nu > 1$ as in (a).

discriminant with discriminants measured from the data, we must evaluate the parameters $(P, \mathcal{L}, h)$ in terms of the shock strength $\alpha\nu$; for example, $P = -2\alpha\nu$, $\mathcal{L}$ is given by the shock compression, and h is determined by the compression and the momentum amplitude. This data fitting is carried out in detail in Appendix E. In particular, for large $\alpha\nu$, we obtain

$$\Delta(\lambda) \cong \frac{\lambda^2 - 2\alpha\nu\lambda - 1}{\alpha\nu}, \quad \alpha\nu \gg 1 \tag{6.11}$$

which is sketched in Fig. 10(a). Notice the location of the spectrum is between $\lambda \in [-1, 1]$ and $\lambda \in [2\alpha\nu - 1, 2\alpha\nu + 1]$, with the large gap between $\lambda = 1$ and $2\alpha\nu - 1$. If we were to consider a chunk of lattice, say, 16 particles wide, which consists of eight, two-particle oscillators periodically repeated, the discriminant may be computed directly from the two-body discriminant.[11] The result is shown in Fig. 10(b). The fact that all extrema of $|\Delta(\lambda)|$ are exactly tangent at ± 2 except for the central peak follows because the excitation is assumed to be strictly a binary one. Only one degree of freedom has been excited in this model, the highest wave-number (binary) excitation. Comparison of this binary discriminant for large $\alpha\nu$ with the measured discriminant

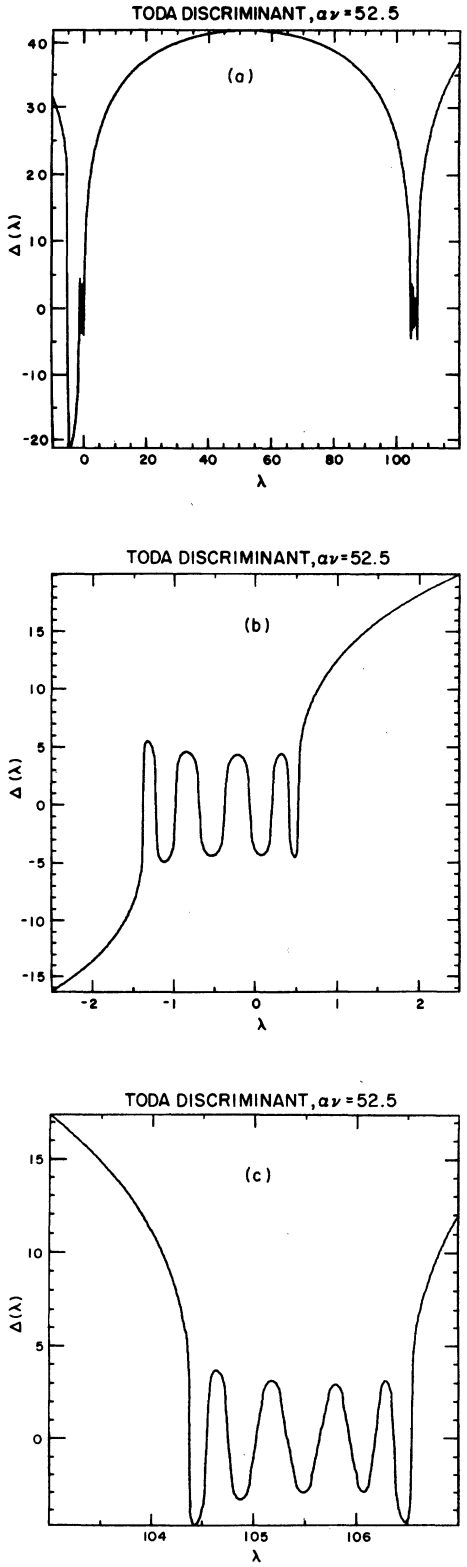

FIG. 11. (a) Discriminant $\Delta(\lambda)$ for $\alpha\nu = 52.5$, $\omega_0 t = 2$, 20 particles near shock front; (b) λ near 0; (c) λ near $2\alpha\nu$.

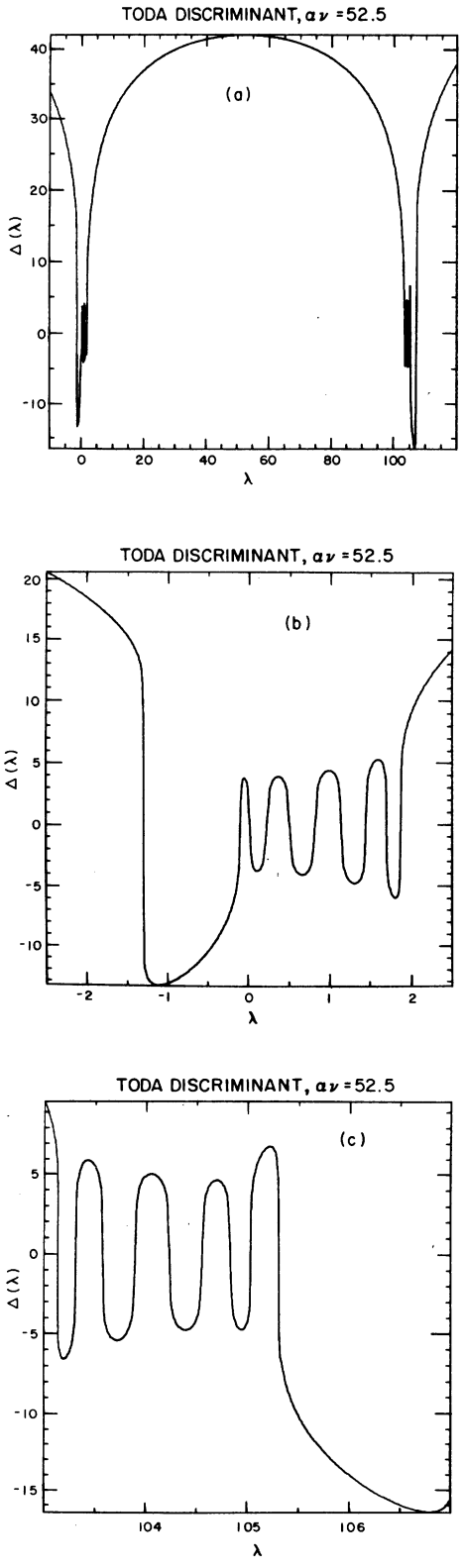

FIG. 12. (a) Discriminant $\Delta(\lambda)$ for $\alpha\nu = 52.5$, $\omega_0 t = 3$, 20 particles near shock front; (b) λ near 0; (c) λ near $2\alpha\nu$.

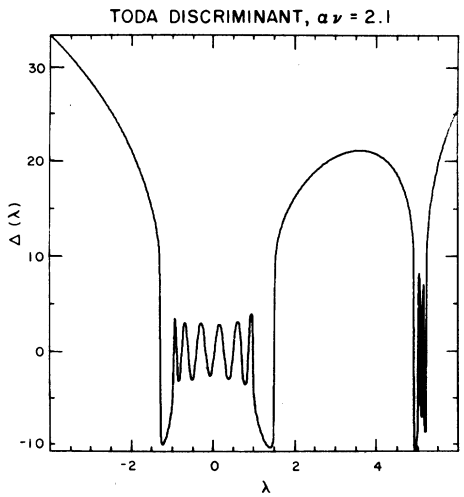

FIG. 13. Discriminant $\Delta(\lambda)$ for $\alpha\nu = 2.1$, $\omega_0 t = 50$, 20 particles near shock front.

for $\alpha\nu = 52.5$ of Fig. 9 shows that the interior of the shock profile away from the shock front is indeed a binary mode.

As one examines chunks of lattice nearer the shock front (for $\alpha\nu = 52.5$), the excitation remains predominantly binary. Figure 11 shows the discriminant for a chunk 20 particles wide, measured from the shock front. Although the central peak is by far the dominant mode in this discriminant, all modes are now excited. According to the rules for reading discriminants,[11] we would interpret this chunk of lattice as containing a packet of supersonic solitons. The soliton packet contains 12 solitons, with λ ranging from 104.5 to 106.5, whose speeds (as calculated by the formula in Ref. 11) are nearly identical and agree with the experimentally measured shock speed of

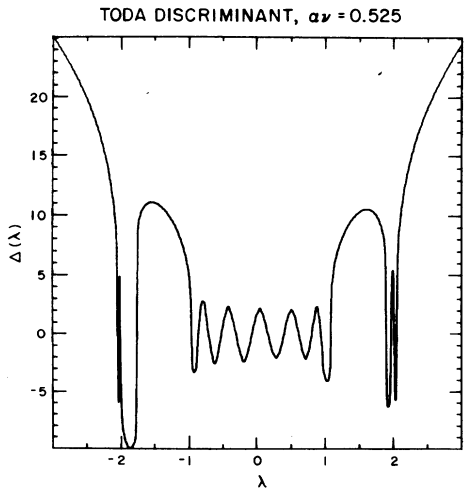

FIG. 14. Discriminant $\Delta(\lambda)$ for $\alpha\nu = 0.525$, $\omega_0 t = 200$, 20 particles near shock front.

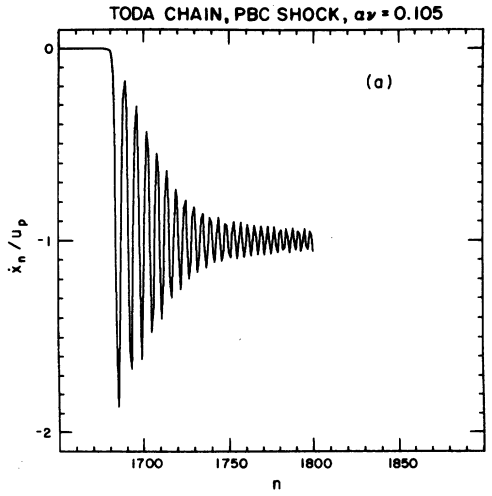

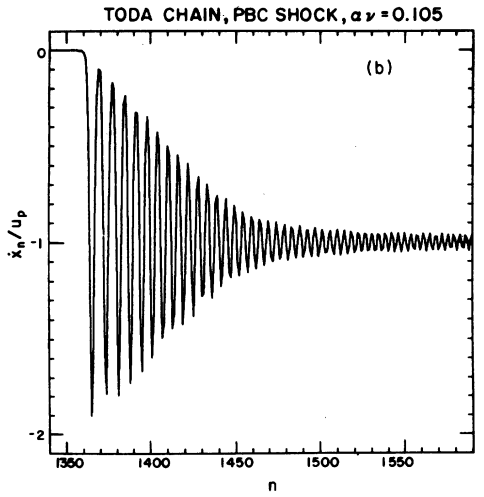

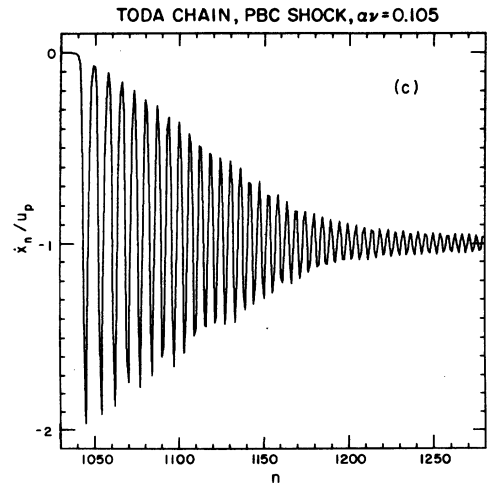

FIG. 15. Particle-velocity $\dot{x}_n/u_p$ profiles vs particle number n for right-running shock wave $\alpha\nu = 0.105$: $\omega_0 t =$ (a) 300, (b) 600, and (c) 900.

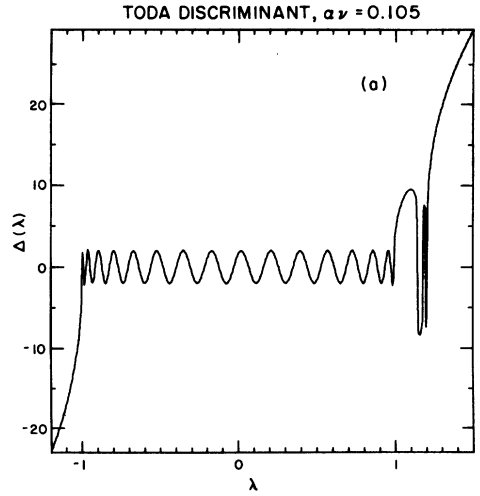

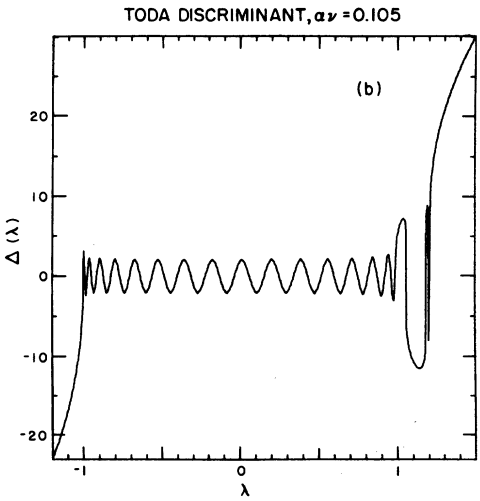

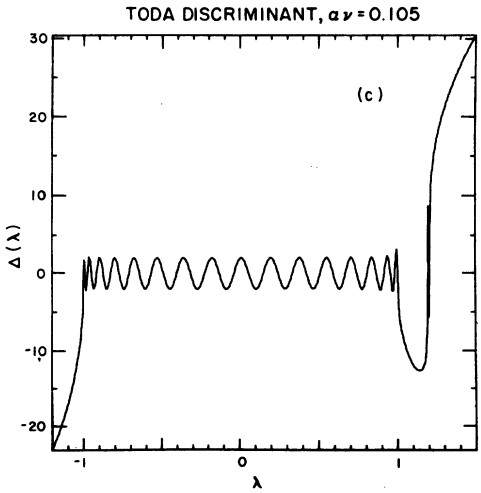

FIG. 16. Discriminant $\Delta(\lambda)$ vs eigenvalue λ for $\alpha\nu = 0.105$, 35 particles at shock front: $\omega_0 t =$ (a) 300, (b) 600, and (c) 900.

$$\mu \cong \frac{2\alpha\nu}{\ln 4\alpha\nu} = 19.7 .$$

These discriminant measurements of the shock profile were taken at time $s=2$. Figure 12 shows the identical measurement at time $s=3$. These figures agree except for the location of the oscillations, which have shifted slightly. This shift is an example of problems which arise when measuring a subsystem which is actually coupled to the full system. In this case the shift arises because the energy of the 20-particle subsystem is not constant. Particle number 20 in the subsystem periodically gives energy to and receives energy from the remainder of the full system through particle number 21. Examination of measured discriminants for times $1 \leq s \leq 1.1$ (in intervals of 0.01) shows that the location of the oscillations in the discriminant experiences small oscillatory behavior with a period which agrees with the vibrational period of the 21st particle.

These discriminant measurements show that, for $\alpha\nu = 52.5$, the shock front is essentially in the binary mode, with the same structure as a packet of solitons.

Figures 13 and 14 continue to examine the shock front for smaller values of $\alpha\nu$ (2.1 and 0.525). In all cases, the front is a packet of solitons whose speeds, as measured from the discriminant, agree with the measured shock speed.

For $\alpha\nu = 0.105$, we illustrate another effect in Figs. 15 and 16. At times $s=300$, 600, and 900, we display the shock profiles and the discriminants for a 35-particle chunk of the shock front. Notice a "tightening" of the soliton packet in the discriminant as s increases from 300 to 900. This tightening means that the leading solitons are approaching equal speeds ($\mu = 1.07$) and equal amplitudes as time increases. This measurement agrees with the flattening of the shock-front profile as s increases (Fig. 15).

Next, we examine the structure of the shock profile as one moves from the shock front, through the transition region, to the rear near the piston. In Fig. 17 we display a sequence of discriminant measurements for $\alpha\nu = 0.525$. According to the rules of Ref. 11, the local wave number increases from $\frac{2}{5}\pi$ to π through this sequence. Using Eq. (6.7), the local compression $\alpha\xi$ can be measured directly from the data as the 20-particle window is moved from the shock front ($n=0$) to near the piston ($n=200$). The following values of $\alpha\xi$ were found: (a) 0.52 ($n=0$), (b) 0.50 ($n=4$), (c) 0.48 ($n=5$), (d) 0.37 ($n=25$), (e) 0.40 ($n=50$), (f) 0.41 ($n=100$), and (g) 0.42 ($n=200$). The average compression from mass conservation [Eq. (2.31)] is $\alpha\xi = \alpha\nu/\mu = 0.395$, which is indeed lower than the local value near the piston (see Sec. V C).

Finally, Figs. 17(g) and 18 compare the rear of the shock near the piston for $\alpha\nu = 0.525$ and 2.1. Both measurements record binary oscillations. The amplitude is very small in the $\alpha\nu = 0.525$ case, while substantial in the $\alpha\nu = 2.1$ case. Notice these two values are on different sides of the critical value $\alpha\nu = 1$; and, indeed, the appearance of the two discriminants is qualitatively different.

We conclude by interpreting these measurements of the structure of the rear of the shock profile through the period-2 or binary discriminant. Recall that in Appendix E we computed the two-body discriminant

$$\Delta(\lambda) = 4\exp(\tfrac{1}{2}\mathcal{L})[(\lambda + \tfrac{1}{2}P)^2 - \tfrac{1}{8}h],$$

and fit its parameters to the data

$$P = -2\alpha\nu,$$

$$\mathcal{L} = \frac{-4\alpha\nu}{\mu(\alpha\nu)}, \tag{6.12}$$

$$h = 8(\alpha\nu - 1)^2\theta(\alpha\nu - 1) + 4\exp(-\tfrac{1}{2}\mathcal{L}),$$

so that

$$\Delta(\lambda) = \begin{cases} 4\lambda^2 - 2, & \alpha\nu = 0 \\ 4(\lambda - 1)^2\exp[-2/\mu(1)] - 2, & \alpha\nu = 1 \\ (\lambda^2 - 2\alpha\nu\lambda - 1)/\alpha\nu, & \alpha\nu \gg 1 . \end{cases} \tag{6.13}$$

Actually, this fit is not quantitatively accurate near $\alpha\nu = 1$ because of the estimate of the local pressure which is used to compute the length $\mathcal{L}$. Nevertheless, it provides qualitative insight from large $\alpha\nu$ through small $\alpha\nu$.

Consider this discriminant as a function of $\alpha\nu$. It is sketched for three values of $\alpha\nu$ in Fig. 19. This quadratic function always has its minimum at $\alpha\nu$. For $\alpha\nu > 1$, the minimum value of Δ is less than two, one degree of freedom (the binary mode) has been excited, and there is a gap in the spectrum. At $\alpha\nu = 1$, the minimum value of Δ reaches -2; no gap exists in the spectrum which ranges from $\lambda = -2$ to 2. As $\alpha\nu$ decreases from 1, the minimum value of Δ remains at -2; the range of the spectrum decreases from $\lambda \in [-2,2]$ to the harmonic limit of $\lambda \in [-1,1]$.

Interpreting the behavior of this binary discriminant, we infer information about the transition through the critical value of $\alpha\nu = 1$. First, this value $\alpha\nu = 1$ is precisely the value at which the gap in the binary spectrum disappears. For $\alpha\nu > 1$, the lattice at the rear of the shock wave experiences finite-amplitude nonlinear binary oscillations which are measured by the width of the central gap in the discriminant. At $\alpha\nu = 1$,

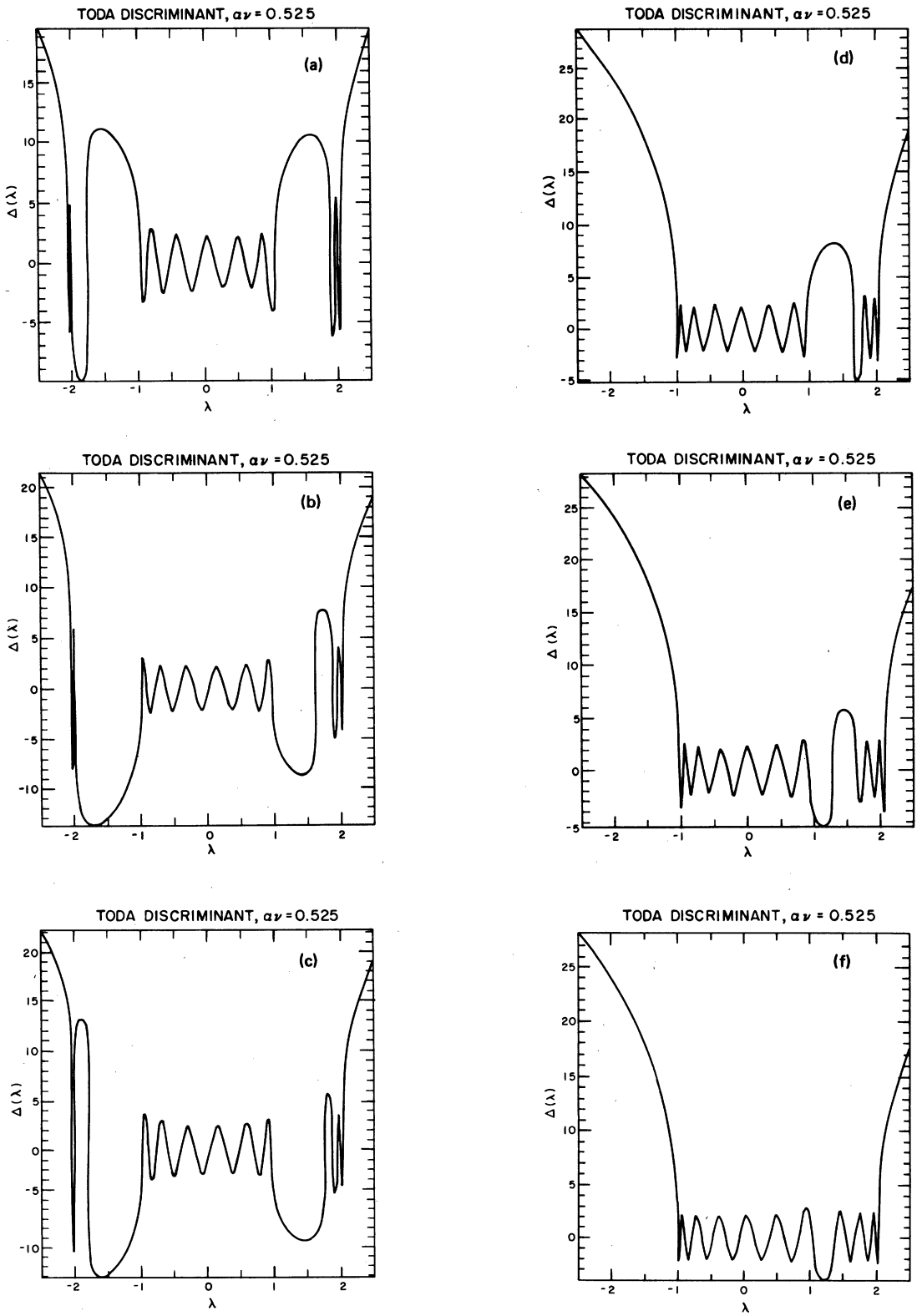

FIG. 17. Twenty-particle discriminants $\Delta(\lambda)$, $\alpha\nu = 0.525$, $\omega_0 t = 200$, for the following number of particles from the shock front: (a) zero (at the front), (b) 4, (c) 5, (d) 25, (e) 50, (f) 100, and (g) 200 (near the piston).

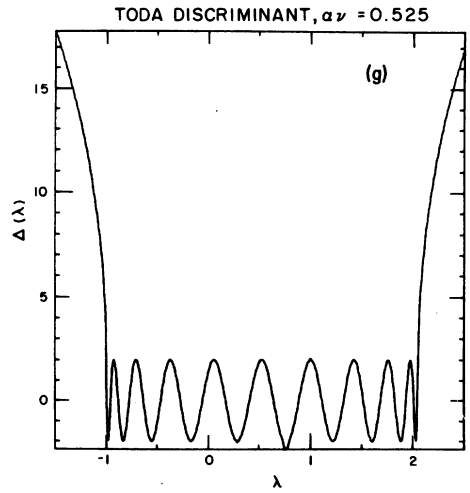

FIG. 17. *(Continued).*

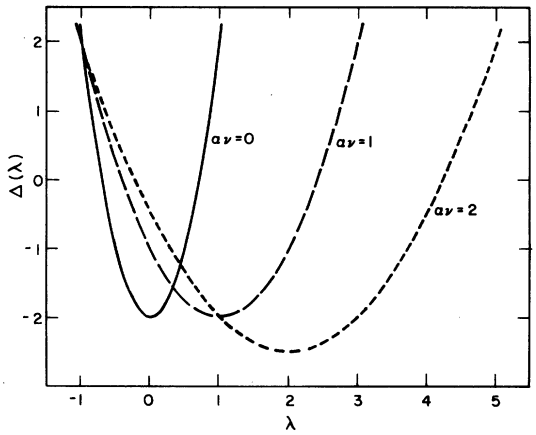

FIG. 19. Binary discriminants $\Delta(\lambda)$ vs eigenvalue λ for shock strengths $\alpha\nu = 0$ (——), 1 (— — —), and 2 (- - -).

the oscillation amplitude becomes infinitesimal as measured by the vanishing of the central bump in Δ and the disappearance of its gap. At this stage, the small-amplitude oscillation is still not harmonic, but it is quasiharmonic because the rear of the shock wave is still under increased effective pressure. This effect appears in the discriminant as spectrum ranging from $\lambda = -2$ to 2, rather than spectrum running over the harmonic range $\lambda \in [-1, 1]$. As $\alpha\nu$ continues to decrease, the local pressure relaxes and the discriminant approaches that of the harmonic excitation.

Thus, we have used the periodic spectral transform to measure the local structure of the shock profile near the rear of the shock wave. The interpretation of these measurements confirms the mechanism for the critical point $\alpha\nu = 1$ as a transition from finite-amplitude nonlinear high-frequency (binary) oscillations to small-amplitude quasilinear high-frequency oscillations. The latter thermalize. This local measurement, using the periodic transform, provides information about the transition which complements that obtained above from the global measurement of the entire shock profile, namely, by the spectral transform under step boundary conditions.

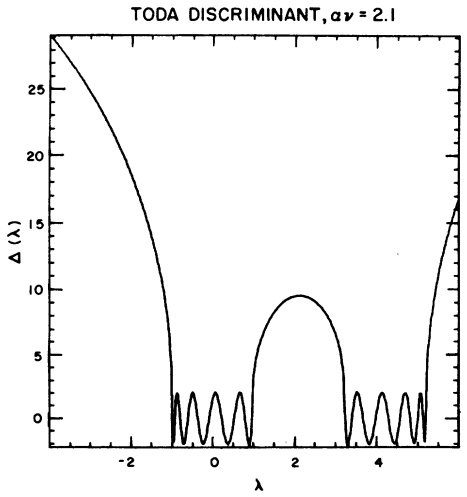

FIG. 18. Discriminant $\Delta(\lambda)$ for $\alpha\nu = 2.1$, 20 particles near the piston at $\omega_0 t = 50$.

ACKNOWLEDGMENTS

We would like to thank J. D. Johnson, Galen Straub, and David Campbell for their helpful comments in discussion of this work. The studies were performed in most part under the auspices of the U. S. Department of Energy. The work of H. Flaschka was supported in part by the NSF under Grant No. MPS 75-07530 and in part by the ARO Grant No. DAAG-29-81-K-0025. The work of D. W. McLaughlin was supported in part by the NSF under Grant No. MPS 75-07530.

APPENDIX A: DERIVATION OF THE KORTEWEG-de VRIES EQUATION FROM THE CONTINUUM EQUATION OF MOTION

The equation of motion in the long-wavelength [small-wave-number ($k \to 0$) or continuum approximation] is, to quadratic degree in q (cubic anharmonicity),

$$\ddot{q} - q'' - \tfrac{1}{12} q'''' + q' q'' \cong 0 , \tag{A1}$$

and the self-consistency requirement in constructing left- and right-running solutions is

$$(q')^{\cdot} - (\dot{q})' \cong 0 . \tag{A2}$$

The linear problem has left- and right-running solutions represented, respectively, by

$$u=\tfrac{1}{2}(\dot{q}+q'),\qquad p=\tfrac{1}{2}(\dot{q}-q'), \tag{A3a}$$

or

$$\dot{q}=u+p,\qquad q'=u-p. \tag{A3b}$$

The equation of motion and self-consistency relation are given by

$$(\dot{u}+\dot{p})-(u'-p')-\tfrac{1}{12}(u'''-p''')\cong 0, \tag{A4a}$$

$$(\dot{u}-\dot{p})-(u'+p')\cong 0. \tag{A4b}$$

The sum and difference of the above pair of equations are then written

$$\dot{u}-u'-\tfrac{1}{24}(u'''-p''')\cong 0, \tag{A5a}$$

$$\dot{p}+p'-\tfrac{1}{24}(u'''-p''')\cong 0. \tag{A5b}$$

For a right-running wave

$$u\cong 0,\qquad q'\cong-\dot{q},\qquad p\cong\dot{q}, \tag{A6}$$

and Eq. (A5b) becomes

$$\dot{p}+p'+\tfrac{1}{24}p'''\cong 0, \tag{A7}$$

the linear Korteweg–de Vries (KdV) equation. An estimate of the error involved in the separation into left- and right-running waves is seen by setting $u\cong 0$ in Eq. (A5a), whence $\frac{1}{24}p'''\cong 0$ indicates when Eq. (A7) is the appropriate first-order (in time derivative) approximation to the second-order linear equation of motion. Note further, that a harmonic right-running solution to Eq. (A7) can be constructed as

$$p(n,s)=\hat{p}\exp[i(kn-\omega s)], \tag{A8}$$

where $k=2\pi/\lambda$ is the wave number (λ = wavelength), $\omega=2\pi/\tau$ is the frequency (τ = period), $\mu=\omega/k=\lambda/\tau$ is the phase velocity, and $\hat{p}$ is the amplitude of the momentum field. From Eq. (A7) we have

$$i(-\omega+k-\tfrac{1}{24}k^3)p\cong 0, \tag{A9}$$

which gives the linear dispersion relationship of frequency to wave number,

$$\omega=k-\tfrac{1}{24}k^3, \tag{A10}$$

as well as the dependence of phase velocity on wave number,

$$\mu=1-\tfrac{1}{24}k^2. \tag{A11}$$

For comparison, consider the discrete harmonic chain, whose dispersion relation and phase velocity are given by

$$\omega=2\sin\frac{k}{2}=k-\tfrac{1}{24}k^3+\cdots,\qquad \mu=\frac{\sin(k/2)}{(k/2)}=1-\tfrac{1}{24}k^2+\cdots. \tag{A12}$$

Thus, the continuum approximation, represented by the linear KdV equation, agrees in the long-wavelength limit ($k\to 0$) with the discrete harmonic chain results.

The nonlinear equation of motion leads, in the same way, to the nonlinear KdV equation

$$\dot{p}+p'+\tfrac{1}{24}p'''+\tfrac{1}{2}pp'\cong 0. \tag{A13}$$

If the above linear left- and right-running solutions of Eq. (A3) are perturbed in the following manner[5]:

$$u=\tfrac{1}{2}[\dot{q}+q'(1-\tfrac{1}{4}q'+\cdots)],\qquad p=\tfrac{1}{2}[\dot{q}-q'(1-\tfrac{1}{4}q'+\cdots)], \tag{A14}$$

then a more accurate separation is obtained, with the error being given by $\frac{1}{24}p'''\cong 0$, just as in the linear case. The nonlinear dispersion relation is more complicated than in the linear case. The canonical form of the nonlinear KdV equation

$$\dot{v}+6vv'+v'''=0 \tag{A15}$$

can be obtained from Eq. (A13) by the transformation

$$p(n,s)=v(2^{1/2}(n-s),72^{-1/2}s). \tag{A16}$$

APPENDIX B: THE CONTINUUM SOLITON

A steady-wave solution of the continuum equation of motion

$$\ddot{q}=q''+\tfrac{1}{12}q''''-q'q''+\tfrac{1}{2}q'^2q''+\cdots, \tag{B1}$$

can be found for the transformed time variable

$$\theta=s-n/\mu, \tag{B2}$$

where μ is the wave speed. With the momentum p defined by

$$\dot{q}(n,s)=p(\theta),\qquad q'(n,s)=-\mu^{-1}p(\theta), \tag{B3}$$

the equation of motion becomes

$$\dot{p}=\mu^{-2}\dot{p}+(12\mu^4)^{-1}\dddot{p}+\mu^{-3}p\dot{p}+(2\mu^4)^{-1}p^2\dot{p}+\cdots. \tag{B4}$$

Integrating by parts, with the condition that the initial momentum $p(-\infty)=0$,

$$\int_{-\infty}^{\theta} dt p^n(t)\dot{p}(t) = p^{n+1}(\theta) - p^{n+1}(-\infty) - n\int_{-\infty}^{\theta} dt p^n(t)\dot{p}(t) = \frac{1}{n+1} p^{n+1}(\theta), \tag{B5}$$

one obtains a new equation of motion

$$\ddot{p} = 12\mu^2(\mu^2-1)p - 6\mu p^2 - 2p^3 = -\frac{\partial \Psi(p)}{\partial p}, \tag{B6}$$

where

$$\Psi(p) = \tfrac{1}{2}p^4 + 2\mu p^3 - 6\mu^2(\mu^2-1)p^2. \tag{B7}$$

Notice that Eq. (B6) is the equation of motion of a pseudoparticle of unit mass in "space" p and "time" θ moving on a pseudopotential surface $\Psi(p)$, whose powers of p correspond to powers of relative displacement in the Hamiltonian of the discrete chain (in the above case, quartic anharmonicity has been included). If the pseudoparticle is given the slightest rightward nudge at time $\theta = -\infty$ when it is sitting at momentum position $p = 0$, it will roll down the potential hill and climb up to amplitude $p = A$ at time $\theta = 0$, where $\Psi(A) = 0$, then roll back down to $p = 0$ at $\theta = +\infty$. This single pulse is a continuum soliton whose speed as a function of amplitude A is

$$\mu = [1 + \tfrac{1}{3}(A/\mu) + \tfrac{1}{12}(A/\mu)^2]^{1/2} = 1 + \tfrac{1}{6}A + O(A^3). \tag{B8}$$

The conservation of pseudoenergy allows one to calculate the full width at half maximum w:

$$\tfrac{1}{2}\dot{p}^2(\theta) + \Psi(p) = 0, \tag{B9}$$

which gives a temporal width

$$\theta = 2\int_{A/2}^{A} \frac{dp}{[-2\Psi(p)]^{1/2}}, \tag{B10}$$

whence

$$w = \mu\theta. \tag{B11}$$

For small amplitude A, where only cubic anharmonicity is important,

$$A = 3\mu(\mu^2-1) \tag{B12}$$

and

$$\Psi(p) = 2\mu p^2(p-A), \tag{B13}$$

so that

$$\theta = 2\int_{A/2}^{A} dp \frac{1}{2\mu^{1/2}p(A-p)^{1/2}} = (A\mu)^{-1/2}\int_{1/2}^{1} \frac{dx}{x(1-x)^{1/2}}$$

$$= (A\mu)^{-1/2}[-2\tanh^{-1}(1-1)^{1/2} + 2\tanh^{-1}(1-\tfrac{1}{2})^{1/2}] = (A\mu)^{-1/2}\ln\frac{1+2^{-1/2}}{1-2^{-1/2}} = \frac{\ln(3+\sqrt{8})}{(A\mu)^{1/2}} \tag{B14}$$

and hence (since $\mu = 1 + A/6 + \cdots$)

$$w = \frac{\ln(3+\sqrt{8})}{\sqrt{A}} + \cdots. \tag{B15}$$

These results show that the continuum soliton reduces to the KdV soliton for sufficiently small amplitudes [see Eqs. (2.13) and (2.14)].

It is clear from inspection of the form of the pseudopotential $\Psi(p)$ that the existence of the steady-pulse continuum soliton is due to a balance between the sharpening effect of anharmonicity and the broadening effect of linear dispersion. (The linear chain will not support a finite-amplitude steady wave.) It is also clear that there is no steady wave allowed with initial momentum $p(-\infty) = 0$ and final steady momentum $p(+\infty) = A \neq 0$. Only the single, isolated pulse is allowed.

APPENDIX C: DERIVATION OF THE BINARY-COLLISION FREQUENCY

For a two-particle ($N = 2$) periodic system under compression ξ, so that time is rescaled according to $\hat{s} = s\exp(\alpha\xi)$ [see Eq. (2.30)], the boundary conditions are [see Eq. (2.27)]

$$q_{n+2}(\hat{s}) = q_n(\hat{s}), \tag{C1}$$

the equations of motion, with $p_n = \dot{q}_n$, are [see Eq. (2.20)]

$$\begin{aligned} \dot{p}_1(\hat{s}) &= \ddot{q}_1(\hat{s}) = \exp(q_0 - q_1) - \exp(q_1 - q_2) \\ &= -2\sinh(q_1 - q_2), \\ \dot{p}_2(\hat{s}) &= \ddot{q}_2(\hat{s}) = \exp(q_1 - q_2) - \exp(q_2 - q_3) \\ &= 2\sinh(q_1 - q_2) = -\dot{p}_1(\hat{s}), \end{aligned} \tag{C2}$$

and the total energy (Hamiltonian) is [see Eq. (2.19)]

$$h_{\text{tot}} = \tfrac{1}{2}(\dot{q}_1^2 + \dot{q}_2^2) + \exp(q_1 - q_2) + q_2 - q_1 - 1 + \exp(q_2 - q_1) + q_1 - q_2 - 1 = \tfrac{1}{2}(\dot{q}_1^2 + \dot{q}_2^2) + 2[\cosh(q_1 - q_2) - 1]. \tag{C3}$$

The center-of-mass coordinate Q and momentum P are

$$Q = \tfrac{1}{2}(q_1 + q_2), \qquad P = \tfrac{1}{2}(p_1 + p_2) = \dot{Q}, \tag{C4}$$

and the relative coordinate q and momentum p are

$$q = q_1 - q_2, \qquad p = p_1 - p_2 = \dot{q}. \tag{C5}$$

From the equation of motion, we note immediately that the center-of-mass momentum is a constant

$$\dot{P} = \tfrac{1}{2}(\dot{p}_1 + \dot{p}_2) = 0,$$

so that

$$Q(\hat{s}) = Q(0) + P\hat{s}. \tag{C6}$$

The equation of motion for the relative coordinate is

$$\dot{p} = \ddot{q} = \dot{p}_1 - \dot{p}_2 = -4\sinh q, \tag{C7}$$

which is consistent with the following Hamiltonian for the relative coordinate

$$h = \tfrac{1}{2}p^2 + 4(\cosh q - 1); \tag{C8}$$

that is,

$$\dot{q} = \frac{\partial h}{\partial p} = p, \qquad \dot{p} = -\frac{\partial h}{\partial q} = -4\sinh q,$$

and when $p = q = 0$, $h = 0$. Since

$$\dot{h} = p\dot{p} + 4p\sinh q = 0,$$

h, the relative-coordinate energy, is a constant of the motion.

Let us choose the initial conditions to be

$$q_1(0) = q_2(0), \qquad p_1(0) = -p_2(0) = \tfrac{1}{2}\hat{A},$$

so that

$$q(0) = 0, \qquad p(0) = \hat{A}. \tag{C9}$$

If $A = \dot{q}(s = 0)$ and $\hat{A} = \dot{q}(\hat{s} = 0)$, then by Eq. (2.30),

$$\hat{A} = A\exp(-\alpha\xi). \tag{C10}$$

The relative energy is then

$$h = \tfrac{1}{2}\hat{A}^2,$$

so that by Eq. (C8)

$$p^2(\hat{s}) = \dot{q}^2(\hat{s}) = \hat{A}^2 + 8 - 8\cosh q. \tag{C11}$$

At time $\hat{s} = \frac{1}{4}\hat{S}$, where $\hat{S}$ is the period of the wave train

$$p_1(\tfrac{1}{4}\hat{S}) = p_2(\tfrac{1}{4}\hat{S}) = 0$$

or

$$p(\tfrac{1}{4}\hat{S}) = 0,$$

$$q(\tfrac{1}{4}\hat{S}) = q_{\max} = \cosh^{-1}(1 + \tfrac{1}{8}\hat{A}^2) = \ln[1 + \tfrac{1}{8}\hat{A}^2 + \tfrac{1}{2}\hat{A}(1 + \tfrac{1}{16}\hat{A}^2)^{1/2}]. \tag{C12}$$

Integrating Eq. (C11) from $\hat{s} = 0$ [Eq. (C9)] to $\hat{s} = \frac{1}{4}\hat{S}$ [Eq. (C12)] gives

$$\int_0^{\hat{S}/4} d\hat{s} = \tfrac{1}{4}\hat{S} = \int_0^{q_{\max}} \frac{dq}{(\hat{A}^2 + 8 - 8\cosh q)^{1/2}} = \tfrac{1}{4}S\exp(\alpha\xi) = \frac{1}{4}\frac{2\pi}{\omega}\exp(\alpha\xi) \tag{C15}$$

or

$$\omega = \tfrac{1}{2}\pi\exp(\alpha\xi)\left(\int_0^{q_{\max}} \frac{dq}{(\hat{A}^2 + 8 - 8\cosh q)^{1/2}}\right)^{-1}. \tag{C16}$$

In the limit $A \to 0$, $q_{\max} \to \frac{1}{2}\hat{A}$, and

$$\omega \to \tfrac{1}{2}\pi\exp(\alpha\xi)\left(\int_0^{\hat{A}/2} \frac{dq}{(\hat{A}^2 - 4q^2)^{1/2}}\right)^{-1} = \tfrac{1}{2}\pi\exp(\alpha\xi)\left(\tfrac{1}{2}\int_0^1 \frac{dx}{(1 - x^2)^{1/2}}\right)^{-1} = \pi\exp(\alpha\xi)[\sin^{-1}(1) - \sin^{-1}(0)]^{-1} = 2\exp(\alpha\xi). \tag{C17}$$

Notice that if the Toda potential had been truncated to include only cubic anharmonicity, Eq. (C17) would be exact, just as it would for a purely harmonic potential; however, the inclusion of quartic, or higher order, anharmonicity results in a departure from the quasiharmonic answer in Eq. (C17).

In the limit $A \to \infty$, $q_{\max} \to \ln\frac{1}{4}\hat{A}^2$, and

$$\omega \to \tfrac{1}{2}\pi \exp(\alpha\xi)\left(\int_0^{\ln\hat{A}^2/4} \frac{dq}{(\hat{A}^2 - 4e^q)^{1/2}}\right)^{-1} = \tfrac{1}{2}\pi \exp(\alpha\xi)\hat{A}\left(\int_{4/\hat{A}^2}^1 \frac{dx}{x(1-x)^{1/2}}\right)^{-1}$$

$$= \tfrac{1}{2}\pi \exp(\alpha\xi)\hat{A}\left[-2\tanh^{-1}(1-1)^{1/2} + 2\tanh^{-1}\left(1 - \frac{4}{\hat{A}^2}\right)^{1/2}\right]^{-1}$$

$$= \tfrac{1}{4}\pi \exp(\alpha\xi)\frac{\hat{A}}{\ln\hat{A}} = \tfrac{1}{4}\pi \frac{A}{\ln A - \alpha\xi}\,. \tag{C18}$$

APPENDIX D: CRITICALITY AND MULTIPLICITY OF THE SPECTRUM OF L

In this appendix we derive the change in multiplicity at the critical value described in Sec. VI. It is required to find the spectrum of L, that is, all bounded solutions of the difference equation

$$\tfrac{1}{2}(u_{n-1} + u_{n+1}) = \begin{cases} (\lambda + v)u_n, & n < -1 \\ (\lambda - v)u_n, & n \geq -1\,. \end{cases} \tag{D1}$$

For motivation, consider the analogous problem for the Schrödinger equation

$$\left(-\frac{1}{2}\frac{d^2}{dx^2} + V(x)\right)\psi(x) = E\psi(x),$$

where $V(x) = -1$ for $x < 0$ and $V(x) = 0$ for $x > 0$. For $E > 0$, there exist two bounded eigenfunctions $\psi_1(x, E)$ and $\psi_2(x, E)$ which oscillate at $x = \pm\infty$. For $-1 < E < 0$, there exists one bounded eigenfunction which oscillates at $x = -\infty$ and decays exponentially at $x = +\infty$ (the other eigenfunction blows up exponentially as x goes to $+\infty$). These considerations yield the spectrum of the Schrödinger operator $E \in (-1, \infty)$. For $E \in (0, \infty)$ this spectrum has multiplicity two; for $E \in (-1, 0)$ it has multiplicity one. In this appendix we perform the analogous calculation for the difference equation (D1).

Fix $\lambda \in [-1 + v, 1 + v]$ and define $Z_+^{(1)}$ as the root of

$$\frac{1}{2}\left(Z + \frac{1}{Z}\right) = \lambda + v,$$

which resides in the interior of the unit circle. Let

$$Z_+^{(2)} \equiv 1/Z_+^{(1)}$$

denote the other root (outside the unit circle). As λ approaches any point on the interval $[-1+v, 1+v]$, $Z_+^{(1)}$ approaches a point on the unit circle and $Z_+^{(2)}$ approaches its complex-conjugate point. Similarly, fix $\lambda \in [-1 - v, 1 - v]$, and define $Z_-^{(1,2)}$ as the two roots of

$$\tfrac{1}{2}(Z + 1/Z) = \lambda - v,$$

with the convention $Z_-^{(1)}$ residing in the interior of the circle.

In terms of these functions, we can define two bases of solutions for the difference equation (D1), $\{\phi^{(1)}, \phi^{(2)}\}$ and $\{\psi^{(1)}, \psi^{(2)}\}$:

$$\phi^{(1,2)}(n, \lambda) \equiv \begin{cases} [Z_+^{(1,2)}(\lambda)]^n, & n < -1 \\ A^{(1,2)}(Z_-^{(1)})^n + B^{(1,2)}(Z_-^{(2)})^n, & n \geq -1 \end{cases}$$

$$\psi^{(1,2)}(n, \lambda) \equiv \begin{cases} [Z_-^{(1,2)}(\lambda)]^n, & n \geq -1 \\ C^{(1,2)}(Z_+^{(1)})^n + D^{(1,2)}(Z_+^{(2)})^n, & n < -1\,. \end{cases}$$

Here the constants (A, B, C, and D) are determined from the difference equation (D1) near $n = 0$.

The following decay properties can be established by inspection:

$\phi^{(1)}(n, \lambda)$. As $n \to -\infty$, it blows up unless $\lambda \in [-1 + v, 1 + v]$, and executes bounded oscillations if $\lambda \in [-1 + v, 1 + v]$. As $n \to +\infty$, it blows up unless $\lambda \in [-1 - v, 1 - v]$, in which case it executes bounded oscillations.

$\phi^{(2)}(n, \lambda)$. As $n \to -\infty$, it decays if $\lambda \in [-1 + v, 1 + v]$ and executes bounded oscillations if $\lambda \in [-1 + v, 1 + v]$. As $n \to +\infty$, it blows up unless $\lambda \in [-1 - v, 1 - v]$, in which case it executes bounded oscillations.

$\psi^{(1)}(n, \lambda)$. As $n \to +\infty$, it decays if $\lambda \in [-1 - v, 1 - v]$ and it executes bounded oscillations if $\lambda \in [-1 - v, 1 - v]$. As $n \to -\infty$, it blows up unless $\lambda \in [-1 + v, 1 + v]$, in which case it executes bounded oscillations.

$\psi^{(2)}(n, \lambda)$. As $n \to +\infty$, it blows up unless $\lambda \in [-1 - v, 1 - v]$, in which case it executes bounded oscillations. As $n \to -\infty$, it blows up unless $\lambda \in [-1 + v, 1 + v]$, in which case it executes bounded oscillations.

From these decay properties, we see the following.

(1) If $\lambda \in [-1 + v, 1 + v] \cap [-1 - v, 1 - v]$, *both* $\phi^{(1)}(n, \lambda)$ and $\phi^{(2)}(n, \lambda)$ execute bounded oscillations for all n; hence, λ belongs to the spectrum and has a multiplicity of 2.

(2) If $\lambda\in[-1-v,1-v]$, but not $[-1+v,1+v]$, only $\phi^{(2)}(n,\lambda)$ is bounded for all n. It decays as $n\to-\infty$, and executes bounded oscillations as $n\to+\infty$. λ belongs to the spectrum and has a multiplicity of 1.

(3) If $\lambda\in[-1+v,1+v]$, but not $[-1-v,1-v]$, only $\psi^{(1)}(n,\lambda)$ is bounded for all n. It decays as $n\to+\infty$, and executes bounded oscillations as $n\to-\infty$. λ belongs to the spectrum and has a multiplicity of 1.

(4) If $\lambda\notin[-1+v,1+v]\cup[-1-v,1-v]$, all eigenfunctions are unbounded and λ does not belong to the spectrum.

In this way, we establish the following *fact*: The spectrum of L consists in the union of two intervals

$$[-1-v,1-v]\cup[-1+v,1+v].$$

If λ belongs to the intersection of these intervals, λ has a multiplicity of 2. If λ in the spectrum does not belong to the intersection, it has a multiplicity of 1.

APPENDIX E: THE BINARY DISCRIMINANT

In this appendix, we compute the binary (two-body) discriminant. Consider a periodic two-particle ($N=2$) Toda lattice whose total lattice displacement due to compression ξ [see Eq. (2.29)] is

$$\mathfrak{L}=-4\alpha\xi.$$

The equations of motion are ($p_n=\dot{q}_n$), $n=1,2$:

$$\dot{p}_n=\ddot{q}_n=\exp(q_{n-1}-q_n)-\exp(q_n-q_{n+1}),$$

subject to periodic boundary conditions

$$q_{n+2}=q_n+\mathfrak{L},$$
$$p_{n+2}=p_n.$$

Introducing center-of-mass coordinate $Q=\frac{1}{2}(q_1+q_2)$ and momentum $P=\dot{Q}=\frac{1}{2}(p_1+p_2)$, as well as relative coordinate $q=q_1-q_2$ and momentum $p=\dot{q}=p_1-p_2$, the above equations can be integrated to give the center-of-mass motion

$$Q(s)=Q(0)+Ps,$$

since $\dot{P}=0$ means P is a constant of motion. The relative-coordinate equation of motion

$$\dot{p}=\ddot{q}=-4\exp(-\tfrac{1}{2}\mathfrak{L})\sinh(q+\tfrac{1}{2}\mathfrak{L}),$$

can be integrated to give the relative energy

$$h=\tfrac{1}{2}p^2+4\exp(-\tfrac{1}{2}\mathfrak{L})\cosh(q+\tfrac{1}{2}\mathfrak{L}).$$

Notice, in particular, the parameter P is the center-of-mass momentum, $\mathfrak{L}$ is the lattice displacement, and h is the relative energy.

To compute the discriminant for this two-body Toda lattice, one begins from the difference operator L which is equivalent to the 2×2 matrix [see Eq. (4.4)]:

$$L=\begin{pmatrix} b_1 & (a_1+a_2) \\ (a_1+a_2) & b_2 \end{pmatrix}.$$

The definition of the variables (a_n,b_n) in terms of (q_n,p_n) yields [see Eq. (6.2)]

$$a_1=\tfrac{1}{2}\exp[\tfrac{1}{2}(q_0-q_1)]=\tfrac{1}{2}\exp[-\tfrac{1}{2}(q+\mathfrak{L})],$$
$$a_2=\tfrac{1}{2}\exp(\tfrac{1}{2}q),$$
$$b_1=-\tfrac{1}{2}p_0=-\tfrac{1}{2}p_2=-\tfrac{1}{2}P+\tfrac{1}{4}p,$$
$$b_2=-\tfrac{1}{2}p_1=-\tfrac{1}{2}P-\tfrac{1}{4}p.$$

The two-body "binary" discriminant is thus given by Eqs. (6.6) and (6.7),

$$\Delta(\lambda)=\frac{1}{a_1a_2}\det(\lambda I-L)+2$$
$$=4\exp(\tfrac{1}{2}\mathfrak{L})[(\lambda+\tfrac{1}{2}P)^2-\tfrac{1}{8}h].$$

Finally, we determine the three parameters $(P,\mathfrak{L},h)$ by fitting them to the data. First, for a left-running shock wave,

$$P=-2\alpha\nu,$$

which is the piston velocity, or average particle velocity behind the shock front. Second, the effective shock compression of Eq. (2.31) may be used to fix the total lattice displacement of this binary system

$$\mathfrak{L}=-4\alpha\xi=-\frac{4\alpha\nu}{\mu(\alpha\nu)}.$$

Finally, the relative energy is obtained by choosing the initial conditions

$$q(0)=-\tfrac{1}{2}\mathfrak{L}=q_1(0)-q_2(0)$$
$$=\tfrac{1}{2}[q_0(0)-q_2(0)],$$
$$p(0)=A=p_1(0)-p_2(0),$$

where the relative coordinate is chosen to be the equilibrium value so that the relative momentum is a maximum. The final oscillatory-state momentum amplitude A can be fit for all shock strengths $\alpha\nu$ by Eqs. (5.11) and (5.12)

$$A(\alpha\nu)=4(\alpha\nu-1)\theta(\alpha\nu-1),$$

where θ is the usual heaviside step-function

$$\theta(x)=\begin{cases}0, & x<0\\ 1, & x\geq0.\end{cases}$$

The relative energy h at time $s=0$, and thus for

all times since h is a constant of the motion, is given by

$$h=8(\alpha\nu-1)^2\theta(\alpha\nu-1)+4\exp\left(-\frac{2\alpha\nu}{\mu(\alpha\nu)}\right).$$

The binary discriminant for the long-time oscillatory region near the piston is thus fit to data by the following form:

$$\Delta(\lambda)=4\exp\left(-\frac{2\alpha\nu}{\mu(\alpha\nu)}\right)[(\lambda-\alpha\nu)^2 - (\alpha\nu-1)^2\theta(\alpha\nu-1)]-2.$$

We only list the behavior for large and small $\alpha\nu$ because the estimate of $\mathcal{L}$, which arises from a comparison of the shock speed with the piston speed, assumes the local pressure agrees with the average pressure across the entire shock profile. This assumption, which is accurate for $\alpha\nu \ll 1$ and $\alpha\nu \gg 1$, introduces errors of 10% near $\alpha\nu=1$.

For $\alpha\nu=0$, $\mu=1$ and the harmonic-limit discriminant is

$$\Delta(\lambda)=4\lambda^2-2.$$

For $\alpha\nu \gg 1$, $\mu=2\alpha\nu/\ln 4\alpha\nu$ and the hard-rod-limit discriminant is

$$\Delta(\lambda)=\frac{\lambda^2-2\alpha\nu\lambda-1}{\alpha\nu}.$$

Notice that in any case $\Delta(\lambda)$ is centered at $\lambda=\alpha\nu$. Also, regardless of the errors introduced by the global estimate of compression, the discriminant for $0 \leq \alpha\nu \leq 1$ is always equal to -2 at minimum and for $\alpha\nu \gg 1$ approaches the value

$$\Delta(\alpha\nu)=-\alpha\nu-1/\alpha\nu.$$

---

*Present address: Courant Institute, New York University, 251 Mercer Street, New York, N. Y. 10012.

[1]B. L. Holian and G. K. Straub, Phys. Rev. B 18, 1593 (1978).
[2]G. K. Straub, B. L. Holian, and R. G. Petschek, Phys. Rev. B 19, 4049 (1979).
[3]M. Toda, J. Phys. Soc. Jpn. 22, 431 (1967); see also Ref. 8 for a review article on the Toda chain.
[4]A. V. Gurevich and L. P. Pitaevskii, Zh. Eksp. Teor. Fiz. 65, 590 (1973) [Sov. Phys.—JETP 38, 291 (1974)].
[5](a) N. J. Zabusky, in *Nonlinear Partial Differential Equations*, edited by W. F. Ames (Academic, New York, 1967), pp. 223–258; (b) M. Toda, J. Phys. Soc. Jpn. 23, 501 (1967).
[6]H. Flaschka, Phys. Rev. B 9, 1924 (1974); Prog. Theor. Phys. 51, 703 (1974).
[7]H. Flaschka and D. W. McLaughlin, in *Contact Transformations*, edited by R. Miura (Springer, Berlin, 1976).
[8]M. Toda, Phys. Rep. C 18, 1 (1975).
[9]H. Flaschka and D. W. McLaughlin, Prog. Theor. Phys. 55, 438 (1976).
[10]P. van Moerbecke, Invent. Math. 30, 217 (1975).
[11]W. E. Ferguson, Jr., H. Flaschka, and D. W. McLaughlin, J. Comput. Phys. (to be published).
[12]H. Flaschka (unpublished).